ABSTRACT

Zhang, Yu.

Ab Initio Electronic Structure Calculations For High-K Dielectrics

(Under the direction of Professor Gerald Lucovsky and Professor Jerry L. Whitten)

In current semiconductor industry, continuing improvement in the performance of MOSFET requires aggressive scaling down of the dimensions of CMOS devices. A better capacitance/unit area can be gained as gate oxide thickness decreases. An equivalent oxide thickness (EOT) less than 1.0nm is required according to the 2002 International Technology Roadmap for Semiconductor (ITRS). However, as gate oxide thickness scaling down, tunneling current will increase, which will lower the device performance. SiO_2, as the widely used gate oxide material, has reached its scaling limit due to the high current leakage at this thickness. Non-crystalline alloys of i) group IIIB, IVB and VB TM oxides and ii) first row RE oxides with SiO2 and Al2O3 have been proposed as alternative high-k gate dielectrics for advanced Si devices.

This dissertation addresses differences between the electronic structure of alternative high-k transition metal dielectrics and SiO2. Ab inito calculations, based on small clusters identify unique aspects of electronic structure that are associated with the TM atoms. The lowest conduction band states are derived from atomic d-states of the TM atoms, and are localized on these atoms. Excitations into these states i) from TM core states, ii) from oxygen K1, iii) from oxygen atom derived valence band states, are simulated by using ab inito calculations at self-consistant-field (SCF) Hartree-Fock and Configuration Interaction (CI)

level. And these electronic structure calculations are used to interpret optical, ultra-violet (UV), X-ray and electron spectroscopies, including UV and X-ray photoemission (UPS and XPS, respectively), and Auger electron spectroscopy (AES), and also provide a basis for interpretation of electrical results and narrowing the field of possible replacement dielectrics for advanced semiconductor devices.

Ab Initio Electronic Structure Calculations For High-K Dielectrics

by

Yu Zhang

A dissertation submitted to the Graduate Faculty of
North Carolina State University
in partial fulfillment of the
requirements for the Degree of
Doctor of Philosophy

Physics

Raleigh, North Carolina

December 2004

APPROVED BY:

Dr. Gerald Lucovsky Chair of Advisory Committee	Dr. Jerry L. Whitten
Dr. Dave Aspnes	Dr. Harald Ade

Dedicated to my parents, Zhisen Zhang and Qin Li for their never ending love and sacrifice

Biography

I was born on October 21, 1974 in Jin Lin, P.R.China. Under the affection of my parents, both are physics teachers, I began to love physics since my childhood. In 1997, I completed my bachelor of science in physics at Peking University, Beijing, P.R.China and enter the graduate school at the same university. Two years later, I received the Master of Science degree in Physics under the direction of Dr. Xing Zhu. On August,1999, I enrolled in the Ph.D. program of Physics, North Carolina State University, USA. After one year courses work and the qualification exams, I joined Dr. Lucovsky's research group and began the study of high K gate oxide material and its electronic properties for the next generation semiconductor devices. I completed the requirements of the Doctor of Philosophy degree in Physics at N.C. State University on Dec. 16, 2004.

ACKNOWLEDGMENT

I would like to express my sincere appreciation to my advisory committee members, Dr. Gerald Lucovsky, Dr. Jerry Whitten, and Dr. Dave Aspens. I owe special thanks to my advisor Dr. Lucovsky and co-advisor Dr. Whitten for their guidance and financial support. This work would not have been possible without their help.

My sincere thanks are extended to my former and current colleagues in Dr. Lucovsky group, Bob Johnson, Bruce Rayner, Chris Hinkle, Joon Goo Hong, Nick Stoute and C. Fulton, for their scientific support and friendship.

Moreover, I want to thank my parents for their never ending love and sacrifice, it would have never been possible to succeed in my study since my childhood.

TABLE OF CONTENTS

LIST OF TABLES

LIST OF FIGURES

Chapter 1. Introduction

1.1 Scaling of Gate Oxide and Alternative High Dielectric Constant Gate Materials

Metal-Oxide-Semiconductor-Field-Effect-Transistor (MOSFET) has been the most important device for Ultra-Large-Scale-Integration (ULSI) during the last three decades [1.1]. As shown in Fig. 1.1, the MOS transistor consists of a semiconductor substrate and a top gate electrode, separated by an insulating gate-dielectric film of thickness d. Source and drain are formed at each side with a channel length L, and carriers (electrons in this n-channel FET) can flow from source to drain when the applied gate voltage is sufficiently large. Thermally grown silicon oxide (SiO_2) has been used as a gate dielectric material for integrated circuit (IC) application due to its superior properties, such as (1) the excellent quality of the silicon-silicon dioxide interface, which has a very low density of interface states ~ 1-2 x 10^{10} $(ev\text{-}cm^2)^{-1}$, (2) the large energy gap (~9eV), (3) the high dielectric breakdown strength, and (4) its thermal stability at high temperatures [1.2]. For decades, MOSFET has been aggressively scaled down in order to achieve better performances, and IC density has been quadrupled every three years [1.3-1.5]. According to the 2002 International Technology Roadmap for Semiconductors (ITRS) [1.6], an equivalent oxide thickness (EOT) less than 1.0nm is required for a high performance microprocessor. However, when device size scaling down, a MOSFET suffers many new issues caused mainly by increased lateral and perpendicular electric fields inside the small-geometry MOSFET since the power supply voltage is reduced much less proportionally to d and L in practical circuit scaling. Among them, probably the most serious problem, which is inevitable when the normal electric field increases across the insulator, is the gate leakage current due to tunneling effect. The conventional SiO_2 MOSFET shows high gate leakage current density (1-10 A/cm^2) with a

gate oxide thickness of 13-15 Å, and may not be proper for low power applications because its high direct leakage current reduces the ratio of on-state to off-state current [1.7-1.9]. Experimental gate oxide (SiO_2) tunneling currents for various oxide thicknesses are shown in Figure 1.2 [1.10]. Since SiO_2 have already reached its limit at this point, a practical solution of this problem is seeking another material with high dielectric constant (k) as the substitution of silicon dioxide. High k material will permit the use of physically thicker gate oxide, which providing the possibility for many order of magnitude reductions in direct tunneling, while still maintain the capacitance that is equivalent to SiO_2. The electrical relations of these factors are shown as following. The gate stack of the MOSFET is a simple metal oxide capacitor. For a parallel plate capacitor,

$$C = \varepsilon_0 \, k(A/d) \qquad \text{eqn 1-1}$$

where C is the capacitance, ε_0 is the permittivity of free space, k is the dielectric constant of the gate oxide, A and d is the area and separation between the plates respectively. As we can see from the above equation, device scaling down will decrease the area A, and physical thickness d is also required to be large enough to minimize gate leakage current, both of these factors will cause the capacitance decrease. So the only choice left is to increase dielectric constant k in order to maintain a large C. Widely used in semiconductor research and industry, an equivalent oxide thickness (EOT) for a capacitance corresponding to SiO_2 is defined as following,

$$d_{EOT} = (3.9 / k) \, d_{physical} \qquad \text{eqn 1-2}$$

where $d_{physical}$ is physical thickness of the high dielectric material, 3.9 is the dielectric constant of SiO_2.

The dielectric constant k of an isotropic or cubic medium relative to vacuum is defined as :

$$k = \varepsilon/\varepsilon_0 = 1 + \chi \qquad \text{Eqn 1-3}$$

where ε is the electric permittivity of the medium, χ is called the electric susceptibility of the medum which is defined as :

$$\mathbf{P} = \varepsilon_0 \chi \mathbf{E} \qquad \text{Eqn 1-4}$$

where polarization **P** is defined as the dipole moment per unit volume in the macroscopic field **E**. The polarization of a crystal may be expressed approximately as the product of the polarizabilities of the atoms (α_j) times the local electric field:

$$\mathbf{P} = \sum_j N_j \alpha_j E_{local}(j) \qquad \text{Eqn 1-5}$$

where N_j is the concentration and $\mathbf{E}_{local}(j)$ is the local field at atom sites j which is given by the Lorentz relation:

$$\mathbf{E}_{local} = \mathbf{E} + \frac{1}{3\varepsilon_0}\mathbf{P} \qquad \text{Eqn 1-6}$$

And solve for **P** to find the susceptibility

$$\chi = \frac{\sum N_j \alpha_j}{\varepsilon_0 - \frac{\sum N_j \alpha_j}{3}} \qquad \text{Eqn. 1-7}$$

Eqn 1-3, 1-7 shows that the larger polarizability of the atoms is, the higher dielectric constant k we can get.

There are three contributions to the total polarizability: electronic, ionic and dipolar [1.24]. Electronic polarizability of the atom arises from the displacement of the electron shell relative to a nucleus. The ionic polarizability comes from the displacement of a charged ion

with respect to other ions, which is due to the vibration of lattice. The dipolar polarizability arises from molecules with a permanent electric dipole moment that can change orientation in an applied electric field. The electronic polarizability is the major contribution at optical frequencies since the ionic and dipolar contributions are small at high frequencies due to the inertia of the molecules and ions.

According to Pauling [1.23], Ti^{4+} and Zr^{4+} ions have much larger electronic polarizabilities than Si^{4+} (Zr^{4+}: 0.37, Ti^{4+}: 0.185, Si^{4+}: 0.0165), and this is the reason why ZrO_2 has higher k (k~4) than SiO_2 (k~3) in the high frequency range from infrared to ultraviolet. In the frequency range from zero up through the infrared, the dielectric constant can be written as following:

$$k(\omega) = k(\infty) + \frac{4\pi Nq^2 / M}{\omega_T^2 - \omega^2} \qquad \text{Eqn. 1-8}$$

where $k(\infty)$ is defined as optical dielectric constant, obtained as the square of the optical refractive index, static dielectric constant k(0) is obtained at $\omega = 0$, N is the number of ion pairs of effective charge q and reduced mass M, ω_T is the TO (transverse optical) phonon frequency. ZrO_2 has much higher k (k ~ 22) than SiO_2 (k ~ 4) in this frequency range because of its lower ω_T and large effective charge q.

Non-crystalline alloys of i) group IIIB, IVB and VB TM oxides and ii) first row rare earth (RE) oxide with SiO_2 and Al_2O_3 have been proposed as alternative high-k gate dielectrics for advanced Si devices [1.11, 1.12]. However, decreases in tunneling anticipated from increased physical thickness will be mitigated in part by reductions in effective conduction band offset energies that define the tunneling barrier between the Si substrate and high-k gate dielectric, as illustrated by Eqn. 1-3[1.13].

$$T \sim \exp(-2t[\frac{4\pi^2 m^*}{h} E_b]^{0.5}) \qquad \text{Eqn. 1-9}$$

where T is the tunneling possibility, quantum mechanically though a square barrier of thickness t, with a barrier height of E_b, and tunneling electron mass m^*[1.14], h is the Planck constant. The nature of these conduction band states, extended s-states as in SiO_2, Si oxynitride alloys, and Al_2O_3, contrasted with significantly more localized d-states as in TM and RE oxides, as well their energy relative to the Si conduction band are an important factor in determining the tunneling current [1.15].

1.2 Local Atomic Bonding And Amorphous Morphology

The local atomic bonding of non-crystalline TM/RE oxides and their silicate and aluminate alloys, and complementary medium range order define an amorphous morphology [1.16] for these dielectrics that is qualitatively different compared to SiO_2 and the Si oxynitrides that are currently being used in gate dielectrics. A framework for tracking the evolution of amorphous morphology from SiO_2 and Al_2O_3 to their respective elemental TM/RE oxides has been developed in Ref. [1.11], and provides a basis for understanding the bonding and morphology in TM/RE silicate and aluminate alloys, and in particular the local bonding of the TM/RE atoms that is needed for electronic structure calculations.

This classification scheme is summarized in Table 1.1, where the nature of the amorphous morphology is correlated with i) an average bond ionicity, I_b, using a definition due to Pauling, and ii) the average oxygen atom bonding coordination. At one end of the system are idealized continuous random networks (CRN), exemplified by SiO_2, and at the other the random closed packing (RCP) ions that characterizes an idealized non-crystalline structure for TM/RE elemental oxides [1.16]. Between these two limiting morphologies are

modified or disrupted network structures (MCRN), that are exemplified by bulk silicate glasses, non-crystalline silicate thin films as well a small number of metal and TM oxides, including respectively Al_2O_3, TiO_2 and Ta_2O_5 [1.11].

Oxides and chalcogenides with I_b up to about 47% form covalently-bonded CRNs, in which the constituent atoms have a coordination that equals their primary chemical valence of two for O, S and Se, three for N, P and As, and four for C, Si and Ge. The atomic bonding coordination in these CRNs obeys the so-called 8-N rule [1.16]. The ease of glass formation, as well as low defect densities in thin films and bulk glasses, is correlated with the near equality of the number bonding constraints per atom and the network dimensionality, and has been discussed in detail in a series of seminal papers by Phillips and his coworkers [1.17-1.20].

The second class of non-crystalline dielectrics is MCRNs that include ionic bonding arrangements of metal atoms that modify and disrupt the covalently bonded network structure. This class of dielectrics is characterized by values I_b between about 47% and 67%. The most extensively studied oxides of this group are the silicate alloys, e.g., SiO_2 that has been alloyed with Na_2O, Al_2O_3, TiO_2, ZrO_2, etc., and quenched from the melt [1.20]. This class also includes deposited thin film Al_2O_3, TiO_2 and Ta_2O_5, as well as TM/RE atom silicate and aluminate alloys such as $(Zr(Hf)O_2)_x(SiO_2)_{1-x}$ in the composition range for $x < 0.5$ [1.12]. The non-crystalline range of alloy formation in thin films is increased significantly with respect to what can be obtained in homogeneous, single phase bulk glasses quenched from melt. The average oxygen and metal atom coordinations for the CRNs increase, and therefore deviate from the 8-N rule due to the increasing faction of ionic

bonding. For example, the oxygen atom coordination increases from two in the CRNs to three in the MCRNs.

The third class of non-crystalline oxides has a random close packed ionic amorphous morphology [1.16]. This class of oxides is defined by a Pauling bond ionicity greater than ~67%, and includes TM/RE deposited at low temperatures (<200°C) by plasma deposition, or by sputtering with post-deposition oxidation [1.11]. The coordination of the oxygen atoms in these RCP ionic structures is typically four.

The average oxygen atom coordination varies approximately linearly as a function of the average bond ionicity I_b. The stability against crystallization and/or chemical phase separation without crystallization decreases as the average oxygen atom coordination is increased, and k increases indicating that compromises must be made between thermal stability and maximum attainable values of k.

1.3 Theoretical Approach

It has been demonstrated in previous studies that the valence and conduction band states in TM and RE oxides and their pseudo-binary alloys are associated respectively with non-bonding oxygen-atom 2p states with π symmetry and TM/RE d-states with additional contributions from oxygen-atom 2p π states as well [1.15]. The symmetry character of the d-state levels is determined primarily by the coordination of the TM/RE atom, and the bonding geometry, e.g., octahedral, tetrahedral, etc. [1.21,1.22]. Figure 1.3 indicates schematic energy level diagrams developed for tetrahedrally-bonded Si and a group of TM atoms (Ti, Zr and Hf) with 4, 6 or 8 oxygen atom neighbors. These diagrams represent one-electron states and therefore do not include relatively strong final state or excitonic effects that are associated

with optical, UV and X-ray excitations to localized TM d-states. The major difference between the two energy level diagrams in Fig 1.3 is in the lowest conduction band states. For Si with four O-atoms neighbors these states are derived from Si-atom 3s-states and are extended in character, and for a TM atom such as Zr with eight oxygen atom neighbors they are derived from Zr-atom 4d-states that are localized on the Zr atoms. Higher conduction bands are Zr 5s- and 5p-states. The conduction band states include oxygen-atom 2p contributions as well. In addiction the valence band states also have contributions from the Zr 4d-states.

The theory of this thesis is based on small clusters that emulate the local bonding of TM/RE elemental oxides. The calculations are many-body in character, and done at the Hartree-Fock Self Consistent Field (SCF), and configuration Interaction (CI) levels. The details of these calculations will be presented later in Chapter 3-6.

Figure 1.4 indicates the ground state energies for small clusters $Zr(OH)_4$ and $Ti(OH)_4$ that illustrate the important aspects of the electronic structure. These kind of clusters have been used to determine the energies of conduction band states for excited states in which are associated with: i) X-ray absorption between TM core states with p-type symmetry and conduction band states with d- and s-like symmetries, ii) X-ray absorption between oxygen 1s core states and conduction band states, and iii) optical absorption between the highest valence band states, and conduction band states with d- and s-like symmetries. The theoretical results derived from these small clusters provide a basis for interpretation of spectroscopic data, which in turn provides insights into the interpretation of electrical data that involve the properties of the TM/RE valence and conduction band states.

1.4 Overview of the Dissertation

Chapter 2 will provide a theoretical basis for the simulations, including the self-consistent field and configuration interaction. Source materials preparation, evolution of the small cluster models, and computer/programming setup of simulations will be described in Chapter 3 and 4. Chapter 4 will also present the result of simulations on each small cluster model, as to emulate intra-atom ionization and inter-atom ionization respectively. In chapter 5, some final words with conclusions along with some of the future work will be given.

1.5 Reference and Figures

[1.1] S.M. Sze, Physics of Semiconductor Devices, 2nd Edition. (1981)

[1.2] T. Hori, Gate dielectrics and MOS ULSIs (1997)

[1.3] G.E. Moore, Cramming More Components Onto Integrated Cirsuits, electronics, 38, No.8 (1965)

[1.4] G.E. Moore, Tech. Dig. Int. Electron Device Meet. (1975)

[1.5] G.E. Moore, Lithography and The Future of Moore's Law, SPIE, Vol. 2438 (1995)

[1.6] International Technology Roadmap for Semiconductors (ITRS), 2002 Edition, Dec., 2002, Semiconductor Industry Association

[1.7] G. Timp, A. Agarwal, F. H. Baumann, etc., Tech. Dig. Int. Electron Device Meet. 1997

[1.8] G. Timp, K.K. Bourdelle, J.E. Bower, etc., Tech. Dig. Int. electron Device Meet. 1998

[1.9] G. Timp, J. Bude, K.K. Bourdelle, J. Garno, etc., Tech. Dig. Int. Electron Device Meet. 1999

[1.10] S-H. Lo, D.A. Buchanan, Y. Taur and W. Wang, IEEE Electron Device Letters, Vol. 18, No. 5, p.209 (1997)

[1.11] G. Lucovsky, J. Vac. Sci. Technol. A 19, 1535, (2001)

[1.12] G. Wilk, R.W. Wallace and J.M. Anthony, J. Appl. Physics 89, 5243 (2001)

[1.13] G. Lucovsky, IBM J. Res. And Develop. 43, p.301 (1999)

[1.14] H. Yang, H. Niimi, Y. Wu, G. Lucovsky, J.W. Keister and J.E. Rowe, Microelectronic Engineering 48, 307 (1999)

[1.15] G. Lucovsky, J.L. Whitten and Yu Zhang, Microelectronic Engineering 59, 329 (2001)

[1.16] R. Zallen, The Physics of Amorphous Solids (Johm Wiley and sons, New York, 1983), Chapter 2

[1.17] J.C. Phillips, J. Non-Cryst. Solids 34, 153 (1979)

[1.18] J.C. Phillips, J. Non-Cryst. Solids 43, 37 (1981)

[1.19] G. Lucovsky and J.C. Phillips, J. Non-Cryst. Solids 227, 1221 (1998)

[1.20] J. Phillips and X. Kerner, Solod state commun. 117, 47 (2001)

[1.21] H.B. Gray, Electrons and Chemical Bonding, (1962) Chapter 9.

[1.22] C.J. Ballhausen and J.B. Gray, Molecular Orbital Theory (1964) Chapter 8.

[1.23] L. Pauling, Proc. R. Soc. London A114, 181 (1927)

[1.24] Charles Kittel, Introduction to Solid State Physics, 7th Edition, 1996

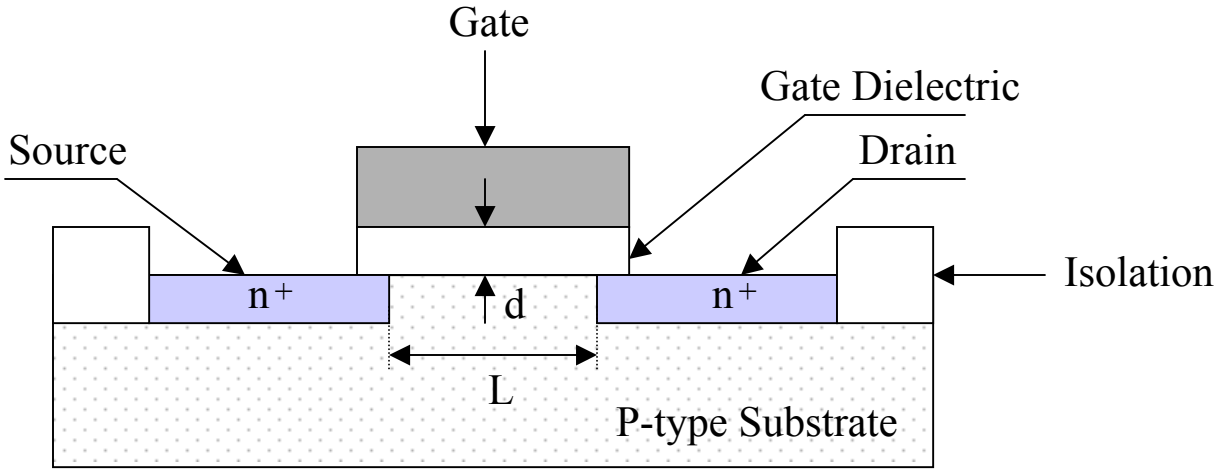

Figure 1.1 Schematic MOS transistor

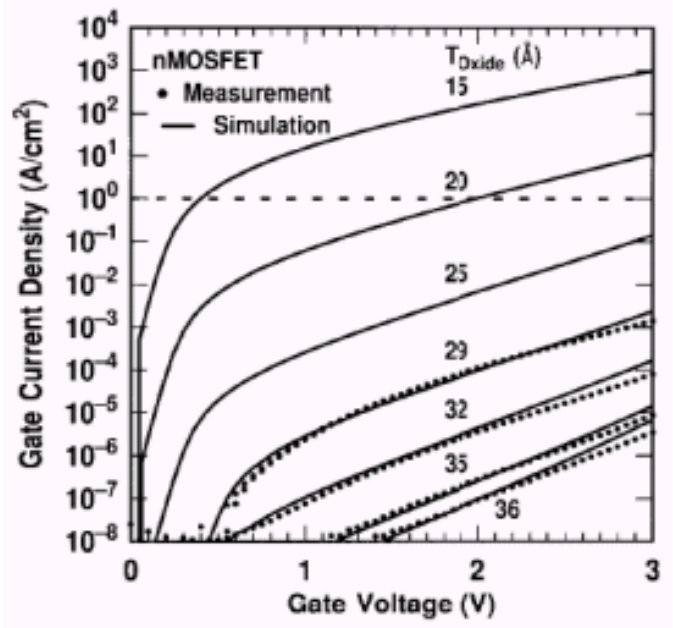

Figure 1.2 Measured and simulated gate leakage currents for SiO2 dielectrics [1.10]

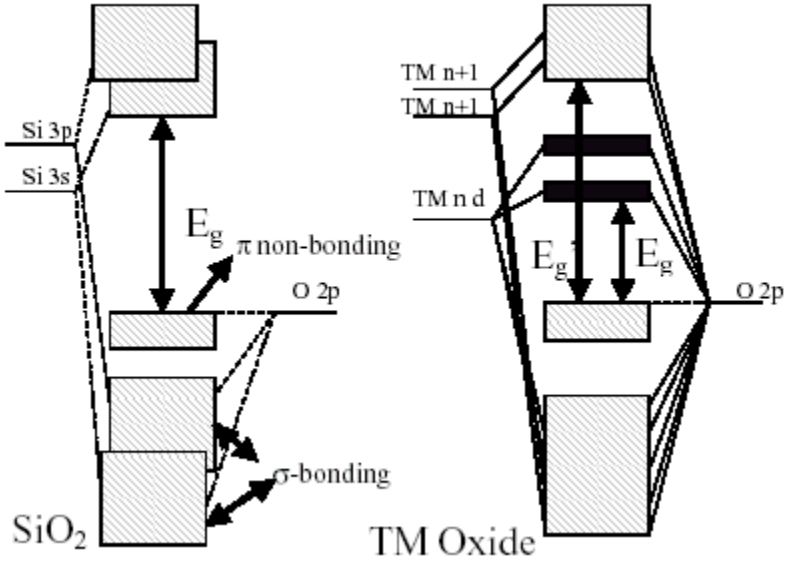

Figure 1.3 Relative orbital energies of SiO2 and group IVB transition metal oxides

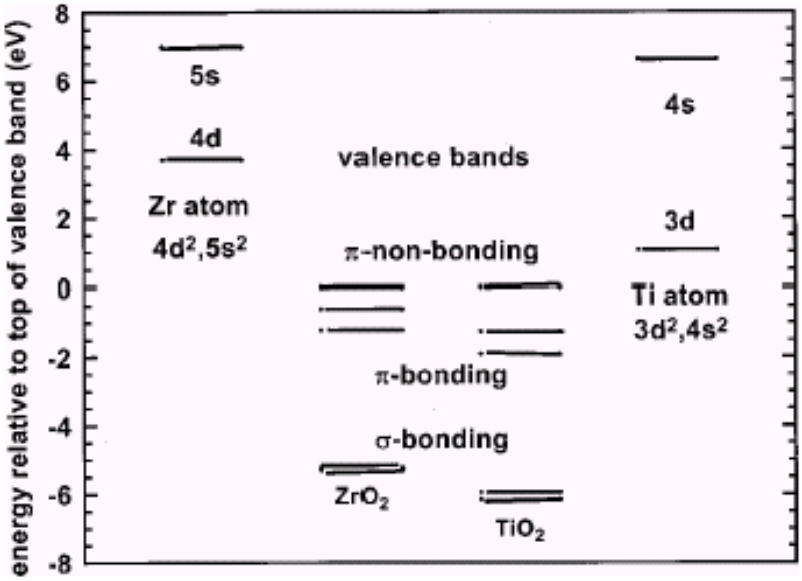

Figure 1.4 atomic state energies and valence band structures for ZrO_2 and TiO_2 from ab initio calculations.

Amorphous Morphology	**Bonding**	**Bond Ionicity**	**Oxygen Atom Coordination**	**Representative dielectrics**
Continuous Random Network -CRN	covalent	< 47%	2	SiO_2, Si oxynitrides
Modified Continuous Random Network -MCRN	covalent with disruption by metal ions	47-67%	increases from 2 to 3	silicate alloys, Al_2O_3, aluminate alloys, Ta_2O_5, TiO_2
Random Close Packing of ions	ionic	> 67%	increases from 3 to 4	TM and REL oxides ZrO_2, HfO_2, etc.

Table 1.1 amorphous bonding morphologies for non-crystalline elemental and binary oxide alloys

Chapter 2. Theory Approach

2.1 The Schrödinger Equation and Wavefunctions [2.1]

All molecular orbital calculations are approximate solutions of the Schrödinger equation:

$$-\frac{\hbar^2}{2m}\nabla^2\psi + V\psi = E\psi \qquad \text{Eqn. 2.1}$$

where ψ gives the profile of the wave associated with a particle of mass m moving in a field of potential V and E is the total energy of the particle, with $\hbar = h/2\pi$, h is the Planck's constant. ∇^2 is the laplacian operator:

$$\nabla^2 = \frac{\partial^2}{\partial x^2} + \frac{\partial^2}{\partial y^2} + \frac{\partial^2}{\partial z^2} \qquad \text{Eqn. 2.2}$$

In a shorthand form, this time-independent Schrödinger equation has always been written as:

$$\mathrm{H}\psi = E\psi \qquad \text{Eqn. 2.3}$$

where H is the hamiltonian operator representing the sum of the kinetic and potential energy of the system. The system we are talking about here is a set of electrons moving in the field of the nuclei.

Equation 2.3 has a series of solutions ψ_i which are *eigenfunctions* (also called "wavefuctions") of the Hamiltonian operator H, and corresponding *eigenvalues* E_i, which are the quantized total energies of the system. The electron density for a one-electron wave or the probability of finding the electron in volume dv is $\psi^2 dv$.

In polar coordinates, the wavefunction is presented as

$$\psi_{nlm}(r,\theta,\phi) = R_{nl}(r)\, Y_{lm}(\theta,\phi) \qquad \text{Eqn. 2.4}$$

where $R_{nl}(r)$ and $Y_{lm}(\theta,\phi)$ governs the radial and angular variation of the wavefunction respectively, and *nlm* are the integral quantum numbers.

2.2 The Hartree-Fock Self-Consistent Fields Method [2.1~2.4]

In molecular orbital theory, the wavefunction for the molecule is an antisymmetrized product of orbitals which has the following form (a single determinant):

$$\psi = (N!)^{-1/2} \det(\chi_1(1), \chi_2(2), \chi_3(3), ..., \chi_N(N)) \qquad \text{Eqn. 2.5}$$

where $\chi_k = \phi_m\alpha$ or $\phi_m\beta$, is a one-electron spin orbital which contains a spin α or β for each orbital. And $\{\chi_k\}$ is an orthonormal set of spin-orbitals:

$$\langle \chi_i(1) \mid \chi_k(1) \rangle = \delta_{ik} \qquad \text{Eqn. 2.6}$$

Each of these one-electron orbitals is itself a complicated linear combination of atomic orbitals:

$$\phi_m = \sum_k c_{mk} F_k \qquad \text{Eqn. 2.7}$$

where the basis $\{F_k\}$ is an orthonormal set of atomic orbitals.

Thus, the solving of Schrödinger equation 2.3 can be broken down into optimizing the coefficients c_{mk} by using the variation principle which requires the calculation of the integrals $\langle \Psi \mid H \mid \Psi \rangle$ and $\langle \Psi \mid \Psi \rangle$.

Assuming all integrals over basis functions $\{F_k\}$ have been evaluated [2.5], the optimization of molecular orbitals with respect to expansion coefficients c_{mk} can be accomplished using the SCF theory of Roothann [2.6]. For the simplest case of closed shell

molecules, where all the electrons are paired with others of opposite spin, the energy expression in terms of integrals over molecular orbitals can be written as:

$$E = \sum_i 2\langle \phi_i \mid h \mid \phi_i \rangle + \sum_i \sum_j \{ \; 2\langle \phi_i(1)\phi_i(1) \mid \frac{1}{r_{12}} \mid \phi_j(2)\phi_j(2) \rangle - \langle \phi_i(1)\phi_j(1) \mid \frac{1}{r_{12}} \mid \phi_i(2)\phi_j(2) \rangle \; \}$$

Eqn. 2.8

which has a compact form:

$$E = \sum_i 2\langle \phi_i \mid h \mid \phi_i \rangle + \sum_{ij} (2J_{ij} - K_{ij}) \qquad \text{Eqn. 2.9}$$

where $h =$ T + V, and the first term is a sum of electron kinetic energy and nuclei-electron attraction, the second and third term represent the coulombic repulsion (J_{ij}) and exchange interaction (K_{ij}) respectively.

The objective is to minimize E with respect to coefficients c_{mk}, while keeping basis set $\{F_k\}$ orthonormal. This can be done by adding Lagrangian multipliers, ε_i, for the normalization constraints to the expression for E. The structure of the equations causes orthogonality requirement to be satisfied.

$$E' = E + \sum_i \varepsilon_i \left(1 - \langle \phi_i \mid \phi_i \rangle\right) \qquad \text{Eqn. 2.10}$$

and $\dfrac{\partial E'}{\partial c_{mk}} = 0$ gives

$$\left\langle F_i(1) \middle| T_1 + V_1 \middle| \chi_k(1) \right\rangle + \left\langle F_i(1)\chi_k(1) \middle| 1/r_{12} \middle| \rho(2) \right\rangle - \left\langle F_i(1)\chi_k(2) \middle| 1/r_{12} \middle| \gamma(1,2) \right\rangle - \varepsilon_k \left\langle F_i(1) \middle| \chi_k(1) \right\rangle = 0$$

Eqn. 2.11

Where ρ is the electron density defined as

$$\rho(1) = |\chi_1(1)|^2 + |\chi_2(1)|^2 + |\chi_3(1)|^2 + \ldots + |\chi_N(1)|^2 \qquad \text{Eqn. 2.12}$$

and $\gamma(1,2)$ is the exchange matrix,

$$\gamma(1,2) = \chi_1(1)\chi_1(2) + \chi_2(1)\chi_2(2) + \chi_3(1)\chi_3(2) + \ldots + \chi_N(1)\chi_N(2) \qquad \text{Eqn. 2.13}$$

Since $\phi_m = \sum_{p'} c_{mp'} F_{p'}$ $\qquad (\chi_k = \phi_m\alpha \text{ or } \phi_m\beta)$

Equation 2.11 becomes

$$\sum_p c_{mp}\left[< F_i(1)|T_1 + V_1|F_p(1) > + < F_i(1)F_p(1)|1/r_{12}|\rho(2) > - < F_i(1)F_p(2)|1/r_{12}|\gamma(1,2) > - \varepsilon_m < F_i(1)|F_p(1) >\right] = 0$$

Eqn. 2.14

or in a much compact form:

$$\sum_p \left(F_{ip} - \varepsilon_m \delta_{ip}\right) c_{mp} = 0 \qquad \text{Eqn. 2.15}$$

The solution of equation 2.15 gives the eigenvalues and eigenvectors of then wavefucntion:

ε_1	ε_2	$\cdots$	ε_m	eigenvalues
c_{11}	c_{21}	$\cdots$	c_{m1}	eigenvectors
c_{12}	c_{22}	$\cdots$	c_{m2}	$\downarrow$
$\vdots$	$\vdots$	$\cdots$	$\vdots$	
c_{1m}	c_{2m}	$\cdots$	c_{mm}	

Eqn. 2.15 is soluble only if

$$\det |F_{ip} - \varepsilon_m \delta_{ip}| = 0 \qquad \text{Eqn. 2.16}$$

and the matrix elements depend on the wavefunctions we are trying to find, so an iteration method has to be used in order to solve this problem. The idea is to use the calculated $\{c_{mp}\}$ to define F_{ip} until self-consistant, i.e., until the eigenvalues and eigenvectors do not changes significantly. Figure 2.1 represents an SCF procedure schematically.

The SCF procedure can be done efficiently by using modern computers. However, some sort of convergence control is also necessary to accelerate the calculations. The most common procedure is to take the energies from successive iterations and to form some

weighted average of the various sets of expansion coefficients. This leads to reduce the oscillatory behavior and helps to avoid divergence. Other factor such as symmetry and initial field may also be an aid to convergence control, i.e., some programs allow the user to specify whether a wavefunction is symmetric or antisymmetric, and a well defined initial field, which usually come from the former simulation, can greatly accelerate the convergence. Generally, convergence is achieved in a number of iterations less than 50.

2.3 Atomic Orbitals and Basis Functions [2.1~2.4]

Since each molecular orbital is a linear combination of atomic orbitals as described in equation 2.7, a good and obvious choice for these atomic orbitals is a set of solutions of the Schrödinger equation for atoms because these will satisfy the requirement for the wavefunction which need to be single valued, finite, continuous, and quadratically integrable.

There are two types of atomic orbitals being used: Slater-type orbitals (STOs) and Gaussian-type orbitals (GTOs). Slater-type orbitals have the form as following:

$$r^{n-1}e^{-\zeta r}Y_{lm}(\theta,\phi) \qquad \text{Eqn. 2.17}$$

which is a solution of the Schrödinger equation for hydrogen-like atoms. ζ is an adjustable parameter which defines the radial part of the orbital along with a power of r, and spherical harmonic $Y_{lm}(\theta,\phi)$ is the angular part of the orbital. So 1s function behaves as $e^{-\zeta r}$, 2p function behave as $re^{-\zeta r}$, and 3d function behaves as $r^2 e^{-\zeta r}$, etc.. These exponents ζ can be optimized by minimizing the totally energy of the system and the conclusions can be understood as an approximate accounting for electron repulsion [2.4]. The numerical choice of exponents is summarized approximately by Slater's rules [2.7]. Although STOs have been used as basis functions for most accurate calculations on atoms and small molecules, it has

two major problems when applied to many-electron atoms or larger molecules: i) the optimum orbitals for many-electron atoms in the single-determinant approximation do not have precisely the same shape as hydrogenic orbitals, and in some cases they are qualitatively different; ii) in a large molecule, the many-centre two-electron integrals are rather difficult which require numerical integration techniques and thus very time consuming [2.2, 2.4]. The Cartesian gausian-type orbitals (GTOs) which have the following form

$$x^l y^m z^n e^{-\alpha r^2} \qquad \text{Eqn. 2.18}$$

have been shown to have sufficient flexibility and to be extremely useful in *ab initio* calculations of polyatomic molecules [2.8~2.11]. By using linear combination of gaussian functions, many-center two-electron integrals can be reduced to much simpler forms since the product of two GTOs is another GTO. In gaussians form, s-functions are taken to behave as $e^{-\alpha r^2}$ where α is the adjustable parameter, p-functions behave as $\mathrm{x}e^{-\alpha r^2}$, $\mathrm{y}e^{-\alpha r^2}$, or $\mathrm{z}e^{-\alpha r^2}$, and d-functions such as d_{xy} behave as $\mathrm{xy}e^{-\alpha r^2}$. The major disadvantage of the GTOs is that it doesn't resemble very closely the form of real atomic orbital wavefunctions especially in the region near the nuclei due to the lack of cusp (as compared with STOs in Figure 2.2), so a large number of functions are needed to provide the best flexibility and accuracy, which will increase the computing time enormously. Several methods had been developed to reduce the basis set [2.2] which will not be presented in this thesis. However, since what we are investigating in this thesis is small cluster molecules consist of many atoms (>30 in some models), Gaussian-type orbitals have been used in all of the calculations and more details will be described in Chapter 3.

2.4 Electron correlation, correlation energy and configuration interaction method

Energies derived by using the Hartree-Fock SCF method are typically in error by 0.5%~1%. Where does this small difference come from? As one may have already noticed in Section 2.2 that a Hartree-Fock wavefunction (Eqn. 2.5) treats the interaction between electrons only in an average way due to the use of a product of one-electron orbitals and having assigned each electron to a particular spatial distribution. However, in reality, the motions of electrons are correlated with each other (electron correlation) and the instantaneous interactions of electrons won't be the same as the average interaction used in the H-F SCF method. Figure 2.3 gives a typical curve of computed SCF energy of a diatomic molecule compared with the true experimental curve. The correlation energy is the difference between the exact nonrelativistic energy and the Hartree-Fock energy.

There are several ways to include the instantaneous electron correlation in calculations, i.e., one of them is to introduce the interelectronic distances r_{ij} into the wavefunction [2.1]. But the most widely used, and probably the most convenient method is the Configuration interaction (CI), also called configuration mixing (CM).

The typical way to do a configuration-interaction calculation is to use the linear combination of the variationally computed SCF orbitals as the new CI wavefunction, then the mixing coefficients are optimized by using linear variational method.

$$\Psi = \sum_i C_i \phi_i \qquad \text{Eqn. 2.19}$$

where ϕ_i is the SCF orbital, C_i is the coefficient, and the new Hamiltonian matrix H is defined under the new basis $\{\phi_i\}$

$$H_{ij} = \langle \phi_i \mid H \mid \phi_j \rangle$$

The processes involved in a SCF_CI calculation are summarized in Figure 2.4.

Although CI method can always provide more accurate energy than SCF does, one thing should be noticed that since the electron correlation depends largely on pair effects, in the cases which are not dominated by two-body interactions, the Hartree-Fock SCF method can give remarkably good result when compared with experiment. Furthermore, SCF computation also can give extremely good answers in cases where one is only interested in the energy differences and no difference in correlation energy between the two situations is to be expected.

2.5 Dipole moment and transition probability [2.12]

When an atom or a molecule makes a quantum jump from a state of higher energy to a state of lower energy, emission of light occurs, and absorption of light takes place by an upward transition from lower state to higher state. The transition probability T(a,b) from state a to state b has the following form:

$$T(a,b) = \frac{64\pi^4\sigma^3}{3h} |\langle a | P | b \rangle|^2 \qquad \text{Eqn. 2.20}$$

where σ is the wave number, and $\boldsymbol{P}$ is the dipole moment expressed in terms of the coordinates of the electrons by the formula:

$$\boldsymbol{P} = -\,\mathrm{e}\sum_i r_i \qquad \text{Eqn. 2.21}$$

In chapter 4, transition probabilities from Ti 2p to 3d* states are calculated using Eqn. 2.20.

2.6 Reference

[2.1] Ira N. Levine, Quantum Chemistry (4th edition), 1991

[2.2] W.G Richards and D.L. Cooper, Ab inito molecular orbital calculations for chemists (2nd Edition), 1983

[2.3] Almon G. Turner, Methods in molecular orbital theory, 1974

[2.4] J.L. Whitten, Ab initio studies of molecules and concepts of molecular structure, Accounts of Chemical Research, 6, 238 (1973)

[2.5] A. C. Wahl, P.E. Cade, and C.C.J. Roothaan, J. Chem. Physics, 41, 2578 (1964)

[2.6] C.C.J. Roothaan, Rev. Mod. Physics, 23, 69 (1951)

[2.7] J. C. Slater, Physics Review, 34, 1293 (1929); 36, 57 (1930)

[2.8] E. Clementi, C. C. J. Roothaan, and M. Yoshimine, Physics Review, 127, 1618 (1962)

[2.9] E. Clementi and D. L. Raimondi, J. Chem. Phys., 38, 2686 (1963)

[2.10] S. Huzinaga, J. Chem. Phys., 42, 1293 (1965)

[2.11] J. L. Whitten, J. Chem. Phys., 44, 359 (1966)

[2.12] E. U. Condon and G. H. Shortley, The theory of Atomic spectra (1935)

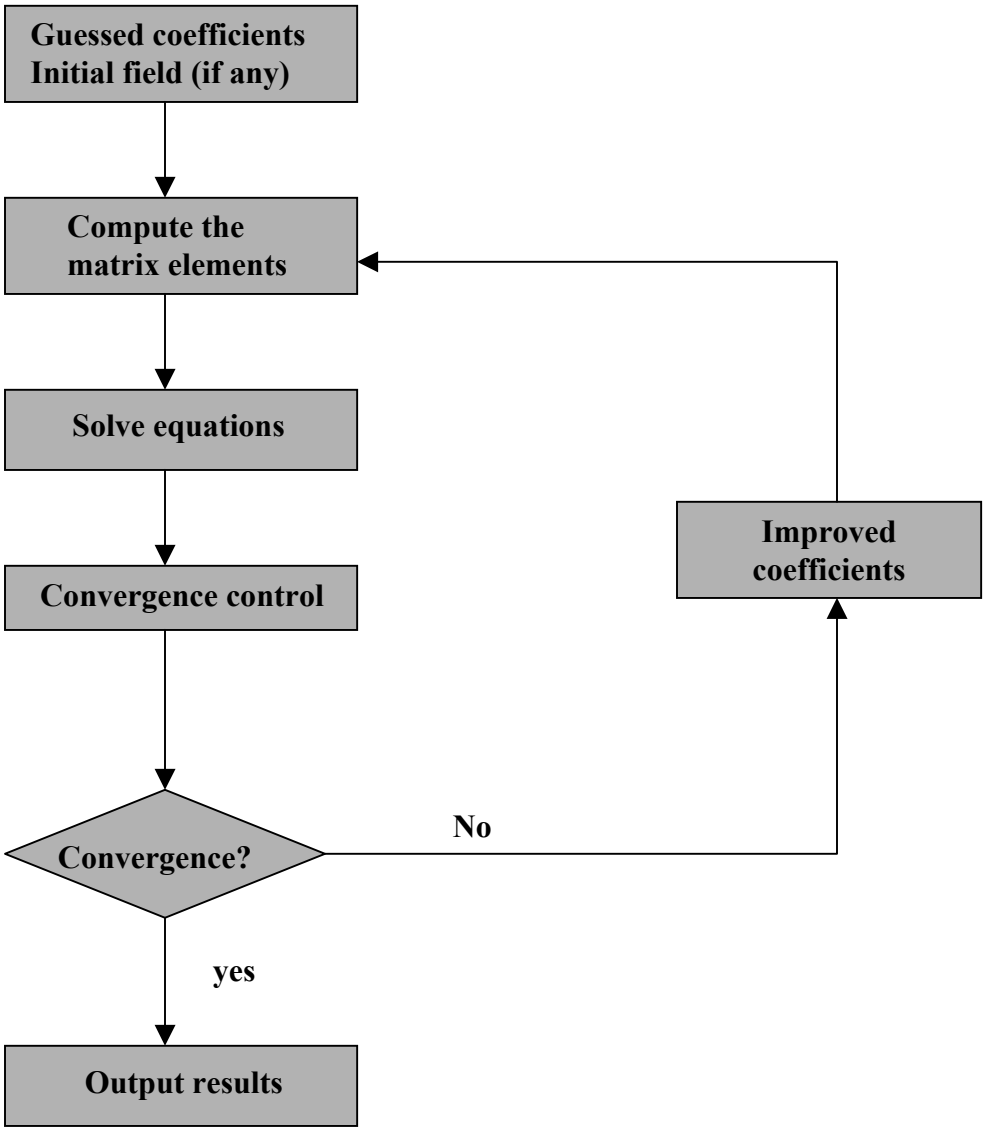

Figure 2.1 Schematic representation of an SCF procedure

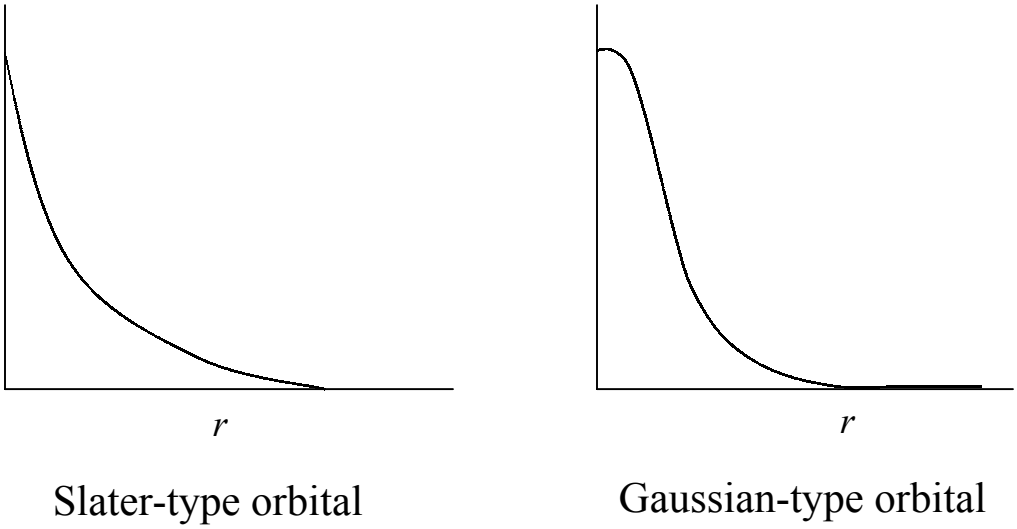

Figure 2.2 different shapes of STO and GTO

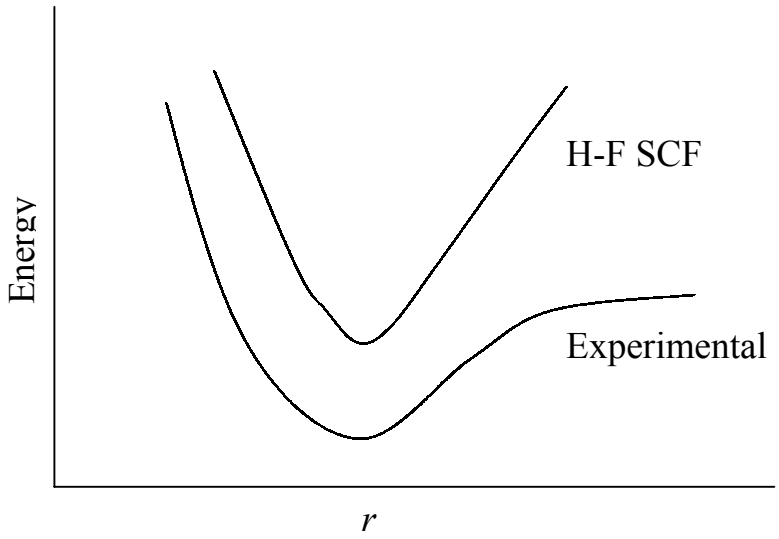

Figure 2.3 comparison of SCF energy and experimental energy of a diatomic molecule

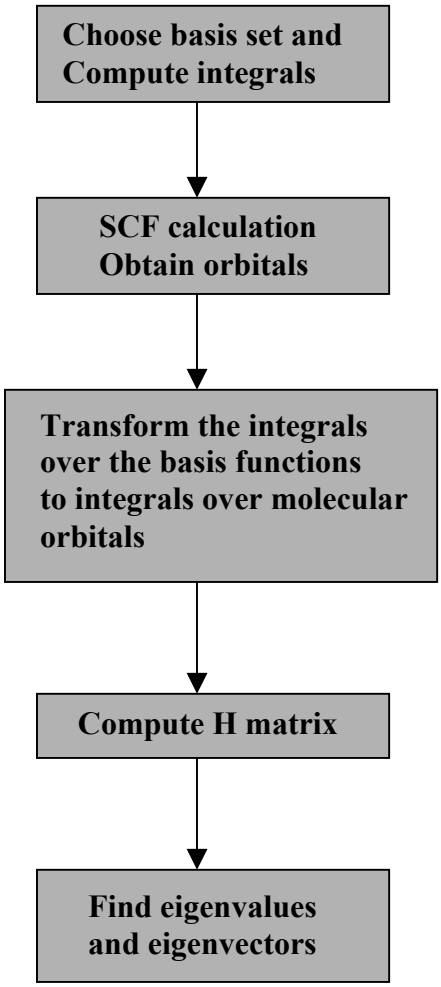

Figure 2.4 Procedure in a SCF-CI calculation

Chapter 3. Material Deposition And Spectroscopic Studies

Works in this chapter (including film deposition) have been done by other members in our/other group, this thesis will only focus on ab inito calculation. Details of sample preparation and spectroscopic study are provided in Reference [3.5~3.9]. Some of the experimental results will be show in Chapter 4 to compare with ab initio calculations.

3.1 Remote Plasma Enhanced Chemical Vapor Deposition (RPECVD)

Transition metal (Zr, Hf, Ti) oxide and silicate alloys were prepared by remote plasma enhanced chemical vapor deposition (RPECVD) [3.1]. For example, Zr silicate alloys were deposited at $300^{\circ}C$ using silane as the Si-atom source gas, and Zr *t*-butoxide as the Zr-atom source gas [3.2]. They were injected downstream from a remote O_2/He (20:1) plasma, and excited O-species extracted from that plasma initiated the CVD deposition process [3.3]. Figure 3.1 gives a schematic description of how RPECVD works. The deposited alloys are fully oxidized, requiring no post-deposition annealing in O-ambients. Substrates were treated in a H_2O/HF (100:1) solution prior to film deposition to remove superficial native oxide. And prior to the Zr silicate alloy deposition, and *a*-SiO_2 layer approximately 3nm thick was deposited on the Si substrate by RPECVD to provide a chemical buffer layer between the Zr silicate and the Si substrate to suppress Zr source gas reactions with the Si substrate. The alloy composition was determined by Rutherford backscattering (RBS) and indicated that the $(ZrO_2)_x(SiO_2)_{1-x}$ alloy films were homogeneous, and fully oxidized with an uncertainty in composition, $\delta x = \pm$ 0.03 [3.4]. The RBS results were used to calibrate on-line Auger electron spectroscopy (AES) results where a linear dependence were demonstrated between the ratio of the derivative spectrum peak-peak heights for $O_{KVV(KLL)}$ and $Zr_{MVV(MNN)}$ features

[3.2], as shown in Figure 3.2 . Hf silicate alloys have also been obtained similarly by RPECVD with two different Hf source materials, $Hf(NO_3)_4$ (Hf_Nitrato) and $Hf[CO(CH_3)_3]_4$ (Hf-t-butoxide).

3.2 XPS, SXPS and XAS

X-ray Photoelectron Spectroscopy (XPS), Soft X-ray Photoelectron Spectroscopy (SXPS) and X-ray Absorption Spectroscopy (XAS) were used to measure O 1s, Zr 3p, Hf 4p, Ti 2p core excitations, and excitations from top of the valence band (O 2p non-bonding states).

3.3 Reference

[3.1] T. Yasuda, Y. Ma, S. Habermehl, and G. Lucovsky, J. Vac. Sci. Tch. B 10, 1884 (1992)

[3.2] G.B. Rayner , D. Kang, Y. Zhang, G. Lucovsky, J. Vac. Sci. Tech. B 20, 1748 (2002)

[3.3] G. Lucovsky, G.B. Rayner, Y. Zhang, G. Appel, J.L. Whitten, Applied Surface Science, 216, 215 (2003)

[3.4] G.B Rayner, R. Therrien, G. Lucovsky, Mater. Res. Soc. Symp. Proc. 611, cl3.1 (2001)

[3.5] C. C. Fulton, G. Lucovsky, and R. J. Nemanich, Appl. Phys. Lett. 84, 580 (2004)

[3.6] Lucovsky G, Hong JG, Fulton CC, et al. JOURNAL OF VACUUM SCIENCE & TECHNOLOGY B 22 (4): 2132-2138 JUL-AUG 2004

[3.7] Hinkle CL, Fulton C, Nemanich RJ, et al., Applied Surface Science 234 (1-4): 240-245 JUL 15 2004

[3.8] Fulton CC, Cook TE, Lucovsky G, et al., Journal of Applied Physics 96 (5): 2665-2673 SEP 1 2004

[3.9] Fulton CC, Lucovsky G, Nemanich RJ, Applied Physics Letters 84 (4): 580-582 JAN 26 2004

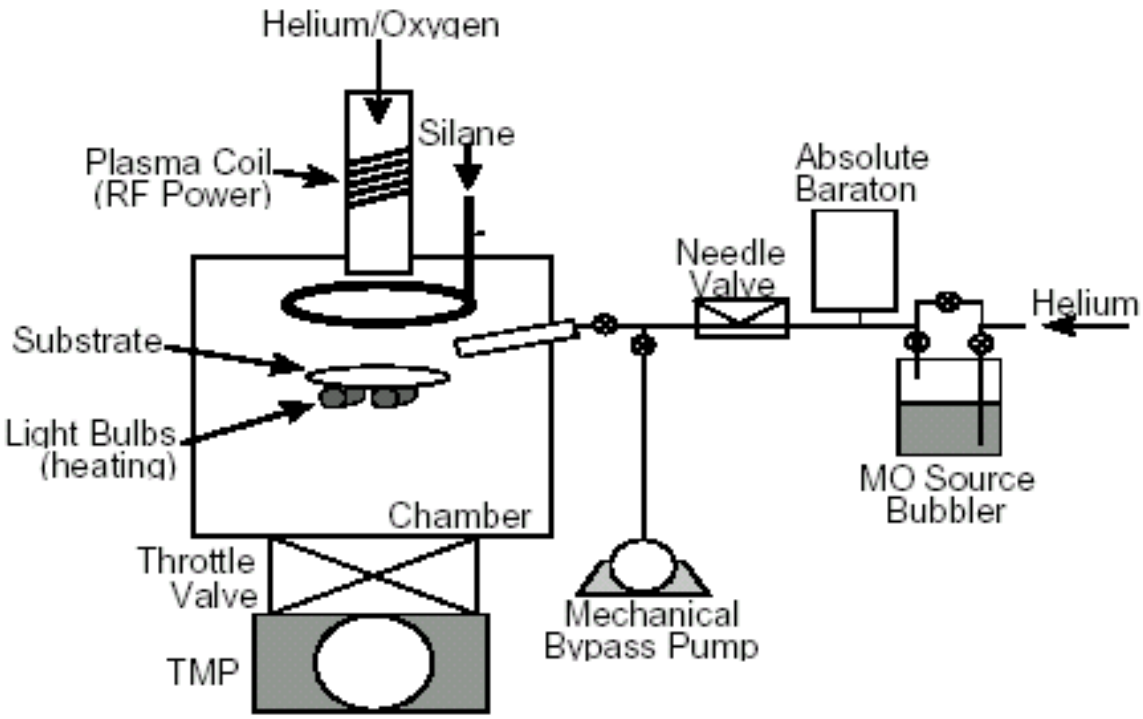

Figure 3.1 RPECVD system [3.1]

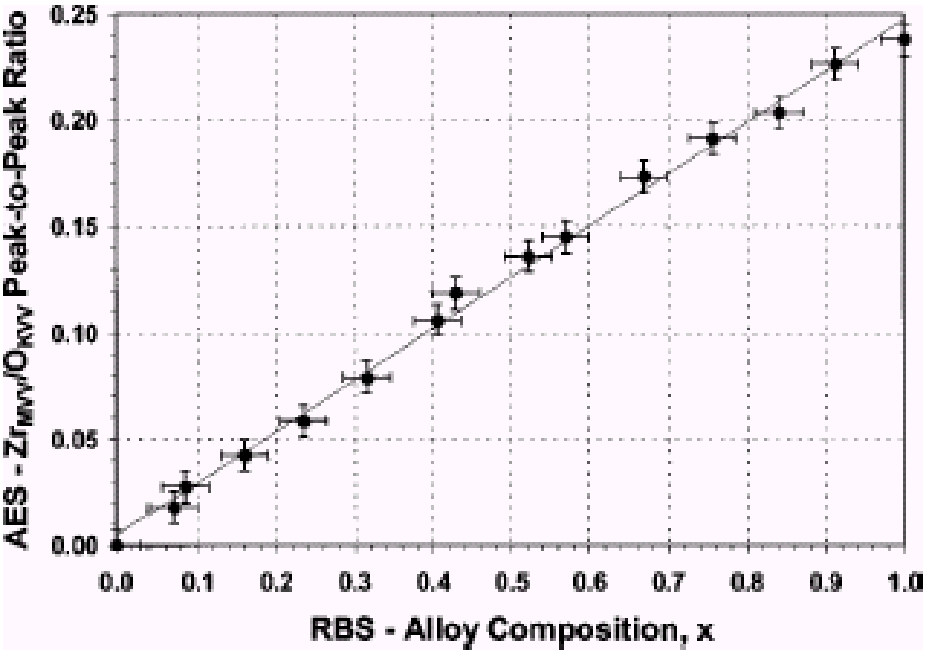

Figure 3.2 Peak height ratio from derivative Zr_{MNN}/O_{KVV} AES as a function of x as determined from RBS studies [3.2]

Chapter 4. *Ab Initio* Calculations

4.1 Simulation Setups

The computer programs used for *ab initio* simulations are provided by Professor Jerry Whitten in Chemistry Department of NC State University. Figure 4.1 shows the programs and procedures for the Self-Consistent-Field (SCF) and Configuration-Interaction (CI) calculation. "datain.dat" is the input file which contains the reference orbitals, basis functions, nuclei and origins. The calculation of all the integrals is done by program "xint", the output is passed to program "xscf" for the calculation of eigenvalues and eigenvectors. Input file "scfinp.dat" is used for convergence control, and also specify the total number of electrons in the molecule such as how many doubly and singly occupied orbitals. "scfout.dat" is the final output of SCF calculation in which we can not only check eigenvalues and eigenvectors, but also electron population in each orbitals. CI calculation consists of 3 step: program "xtrn" translates the integrals from old basis orbitals to new basis which we get from "scfout.dat", then "xci1" generates configuration interactions and "xci2" solves the matrix, final result is given by "ci2out.dat".

The reference orbitals (Gaussian functions) used for description of Zr, Hf, Ti, O, H are listed in Appendix A. Nuclei and origins for each model are listed in Appendix B. Atomic units are used in these simulations. The relationship between the various energy units is shown as following:

1 atomic unit of energy (hartree) = 27.21 eV

1 electron volt = 8065.5 cm^{-1}

1 atomic unit of distance (bohr) = 0.529177 Å

4.2 Crystal Structure Of Transition Metal Oxide

4.2.1 Fluorite-Like Structure (ZrO_2, HfO_2)

Zirconia (ZrO_2) exists in three crystal phases at different temperatures. It exists as a monoclinic crystal at room temperature. At intermediate temperatures (1170°C -2370°C) it has a tetragonal structure. At very high temperatures (>2370°C) the material has a cubic Fluorite structure. Figure 4.2 shows the distribution of the atoms of ZrO_2 (Fluorite) within the unit cube. In this group, each Zr atom is surrounded by eight O atoms, and each O atom has about it a tetrahedron of Zr atoms [4.1]. The Zr atoms themselves form a Face Centered Cubic with 8 Oxygen atoms embedded in each cube. The positions of Zr and O are shown below:

Zr: 000; F.C. O: (¼, ¼, ¼)

The cell dimension *a* is 5.07Å and the distance between Zr atom and its Oxygen neighbors is 2.2 Å correspondingly.

Hafnium dioxide in cubic symmetry has the same kind of crystal structure as ZrO_2 shown above, only with a slightly different cell dimension *a* equal to 5.115 Å. The Hf-O bond length is also close to 2.2 Å.

4.2.2 Rutile-Like Structure (TiO_2)

Titanium dioxide (TiO_2) has three different forms: anatase, brookite, rutile. TiO_2 in rutile symmetry is what we are interested in and investigated in this thesis. Figure 4.3 shows the atomic arrangement of TiO_2 in rutile form. In this group, each Titanium atom is surrounded octahedrally by six Oxygen atoms and each Oxygen atom is terminated by three

Ti atoms. However, this is not an ideal octahedral symmetry since bond-angle θ_1 is not equal to θ_2 (both should be equal to 90° in ideal octahedral), and bond-length a_1 is not equal to a_2 either. The position of atoms are shown blow:

Ti: 000; ½, ½, ½ O: uu0; u+½, ½-u, ½

where parameter u is 0.3053 for TiO_2 (rutile) [4.1]. The cell dimensions, Ti-O bond-length and angels are given in Figure 4.3.

4.3 TM-Centered Small Cluster Models

4.3.1 Four-Fold-Coordination Models (TM atom centered)

As a simple and easy start, the first model we built for the calculation of electronic structure of TM oxide is a four-fold-coordination molecule, as shown in Figure 4.4. In this model, we put the transition metal atom (Zr/Hf/Ti) in the center, which is surrounded by four oxygen atoms in a tetrahedral symmetry. At the boundary of the cluster, a hydrogen atom is used to terminate each oxygen atom. The optimized distance between oxygen and hydrogen atom is 0.97 Å. Bond-length between TM atom and oxygen atom was optimized by minimizing the total SCF energy of the molecule versus different bond-length (Figure 4.5 shows the optimal distance between Zr and O atom is around 1.9 Å~2.0 Å). In this model, Zr/Hf-O bond-length is set to 2.0 Å, and Ti-O bond-length is set to 1.8 Å. The calculated ground states of $Zr(OH)_4$ are presented in Figure 4.6. All these orbitals are doubly occupied with electrons. Since there are four oxygen atoms in this model and each oxygen has three 2p states, the valence band consist of twelve oxygen 2p states which split into two different groups, π and σ. σ group has four O 2p states (one from each oxygen atom) in the direction

of Zr to Oxygen, while the other eight O 2p states form the π group in the direction perpendicular toZr-O. On top of the valence band there are three non-bonding oxygen 2p states, while the rest shows mixing with Zr 4d, 5s and 5p. The unoccupied orbitals (so called "virtual orbitals") above the valence band are not shown in the figure, those are anti-bonding orbitals including Zr 4d, 5s and 5p states which are mixed with oxygen 2p states. Besides the valence band orbitals, Zr 3d, 3p, 3s, 2p, 2s, 1s and O 1s are the core orbitals which has much less orbitals energy than those O 2p state on the top. Zr 4s, 4p, together with O 2s are considered in deep valence band. In Figure 4.7, electronic structures of valence band from $Zr(OH)_4$ and $Ti(OH)_4$ are compared. $Ti(OH)_4$ shows the similar valence band structure as $Zr(OH)_4$, both of them have the oxygen non-bonding states with nearly the same orbital energy. However, as shown in the figure, there is a 2.7eV gap between Zr 4d and Ti 3d in atomic energy levels, which is exactly the difference in reported band gaps for ZrO_2 (~5.6eV) and TiO_2 (~3.0eV).

This model has the same local site symmetry as SiO_2, where Si is surrounded by 4 O in tetrahedral symmetry. In addition, the entire cluster is neutral and has no permanent dipole moment. However, in this model, the TM atom only has 4 O neighbors, which is smaller than the number of oxygen neighbors in the elemental oxides is greater, 6 in TiO_2, and 7 or 8 in ZrO_2 and HfO_2. IN addition the bond angle between the TM, the O-atom and the H-atom has been set at 180° and not equal to the bond angle of terminating OH groups in Si. Finally, O-H bond is significantly more ionic than a TM-O bond.

A slightly better four-fold coordination model is given in figure 4.8, where the Zr, O and H atoms form an angel of 109.5° instead of 180° as shown in Figure 4.4. This model

gives a better description of O 2p states that form the valence band since the oxygen atom is more correctly polarized by its neighbors (Zr and H).

4.3.2 Eight-Fold-Coordination Models (Zr/Hf atom centered)

In order to simulate zirconium/hafnium oxide or zirconium/hafnium silicate in eight-fold symmetry, four water molecules are added into the tetrahedral model (Figure 4.8) so that the central TM atom has totally eight oxygen atoms around it, as shown in Figure 4.9. In this model, central TM atom forms 4 partially covalent bonds to OH groups and 4 donor-acceptor bonds to water molecules. By minimizing the total SCF energy of this cluster, an optimal spacing between Zr and H_2O group was found to be 2.6 Å ~2.7 Å. The calculated total energy versus different bond-length is given in Figure 4.10.

Although the 8-fold coordination model with 4 water molecules inside (Figure 4.9) can provide good description of Zr/Hf silicate, it is not a good model once come to ZrO_2 in cubic symmetry since it is apparently that not all the eight Zr-O bonds are equal to each other. In order to make the eight oxygen atoms equal to the central TM atom, a new model was developed as shown in Figure 4.11. In this model, eight oxygen atoms are placed in each corner of the cube with the same distance to the central TM atom, and a “pseudo” atom is used to terminate each oxygen atom. We use “pseudo” here because it is not a real atom. It has the same basis functions as hydrogen atom does, but with 1.5 positive charge in nuclei instead of 1. The reason for using this “pseudo” atom is that we need to make the whole cluster in neutral and has no permanent dipole moment while still maintain the oxygen 2p states fully filled with electrons. The spacing between oxygen atom and its “pseudo” neighbor is kept as 0.97 Å, which is the optimized O-H distance. A 2.2 Å Zr-O bond-length

is obtained by minimizing the total SCF energy of the cluster as shown in Figure 4.12 , which is exactly the bond-length in real crystal shown in Figure 4.2.

An improved 8-fold coordination model is shown in Figure 4.13, where each oxygen atom is terminated by three "pseudo" atoms in a tetrahedral symmetry together with the central TM atom. Each of the H-like "pseudo" atoms has 0.5 positive charge in nuclei and a distance of 0.97 Å to the oxygen. By splitting the "pseudo" atom in Figure 4.11 into three identical ones, we make oxygen atoms polarized in the correct directions as shown in Figure 4.2.

The model shown in Figure 4.13 is the final TM-centered model we made for the emulation of Zr/Hf oxides, ab inito calculation result and comparison with spectrums will be presented later in this chapter.

4.3.3 Six-Fold-Coordination Models (Ti atom centered)

Since TiO_2 (rutile) has a distorted octahedral symmetry (Figure 4.3), the corresponding small cluster model is built in six-fold-coordination, as shown in Figure 4.14. Again, a total number of 12 H-like "pseudo" atoms are used to terminate oxygen, and each of the "pseudo" atoms has $2/3$ positive charge in nuclei in order to make the whole cluster neutral. By arranging the atoms this way, every oxygen atom is correctly polarized in three different directions. Ti-O bond lengths and angels are given in Figure 4.14, same as those parameters shown in Figure 4.3. Spacing between each oxygen and "pseudo" atom is kept as 0.97 Å.

4.4 Oxygen-Centered Small Cluster Models

Although those TM-centered small cluster models presented in last section have proved to be good description to the real crystal in the TM core excitation (ab inito calculations of TM core excitation will be given later in this chapter), it fails to give the correct answer in the simulation of oxygen core excitation. The deficit of these TM-centered models (Figure 4.13, 4.14) is that only the central transition metal atom has been terminated correctly with real neighbors (oxygen) and the TM-O bonds are in equivalent, while the oxygen is in "poor" description due to the using of "pseudo" atoms as its neighbors, i.e., in ZrO_2 and HfO_2 model (Figure 4.13), only one of the four bonds of O and its neighbors is TM-O bond which is covalent, the other three are O-"H" bonds which are more ionic and very different from TM-O bond. Thus an inaccurate result is inevitable once come to the oxygen core excitation problem.

The solution is to build an oxygen-centered model in which oxygen is terminated by real TM atoms. However, the new model is not easy to build due to several reasons: i) the central oxygen has to be terminated with correct number of TM atoms (4 Zr atoms in ZrO_2, for example), this requires a lot more (>300) basis orbitals to be added which our computer system can hardly handle; ii) each Zr has to be in good description because it is the Zr 4d and 5s states what we are interested in, so that 8 oxygen atoms need to be used to terminate each Zr which make the model even larger; iii) how to terminate those oxygen atoms? Since overall we need to make the whole cluster neutral.

In order to simplify the problem, we first developed a Zr core potential consist of Zr 1s, 2s, 3s, 2p, 3p and 3d. By putting these states in a core potential, the number of basis

orbitals used for a single Zr atom was reduced from 70 to 40. The following procedures were performed in the development of Zr core potential:

i) Determine the smaller expansions by taking the old basis (listed in Appendix A) and allowing all gaussian coefficients to vary, i.e., decontract the s, p and d groups to obtain single gaussians.

ii) Perform full SCF calculation. Proceed by eliminating the smaller coefficient terms.

iii) Use the expansions from ii) to define the orbitals. Obtain the core density using program "xdens2".

iv) Further reduce the size of the atomic orbitals to: S 10 terms, P 6 terms, D 5 terms. And determine a valence basis of 4s, 4p, 5s, 4d. The 4s, 4p can be 10-term and 6-term functions and other should have additional flexibility.

The well developed Zr core potential and atomic orbitals are included in Appendix B.

Similar procedures were performed on oxygen and 1s-2p core potential was obtained, as shown in Appendix B. One thing should be noticed here that we put all three oxygen orbitals (1s, 2s, 2p) into the core potentials so that these oxygen atoms (except the central oxygen) are greatly simplified, which further reduced the total number of basis orbitals required for this model.

Figure 4.15 shows the oxygen-centered small cluster model we built. The central oxygen (in red color) is set to have full basis orbitals (14 in total). Four Zr atoms with reduced basis orbitals (40 each) surround the central oxygen in a tetrahedral symmetry. Each Zr is surrounded by eight "modified" oxygen atoms (22 in total, some of them are shared by different Zr). We call it "modified" because during the simulation we put more than 8

electrons into core potential for each of these oxygen (oxygen will attract electrons from Zr due to its larger electron negativity), then check the number of electrons in the central oxygen after each run and use this number to modify the oxygen in outer shell then run it again. After several iterations a converged point is obtained. Our calculation shows the oxygen has 9.244 electrons at the converged point, and this means the Zr-O bond is about 60% ionized. At the boundary, 24 pseudo charges (+0.557 each) are used to terminate the oxygen and make the whole cluster in neutral.

An oxygen-centered small cluster model was built for TiO_2 (rutile) similarly, as shown in Figure 4.16. The central oxygen (in red color) is surrounded by three Ti atoms, and each of the Ti is surrounded by six "modified" oxygen in a distorted octahedral symmetry. The bond-length and angels used in this model are the same as those in Figure 4.3.

4.5 Comparison Of Ab Initio Calculations Result And Spectroscopy study

4.5.1 Intra-Atomic Excitation

We call it "Intra-atomic excitation" because the electron is excited from one of the core states in the TM (Transition Metal) atom to the higher unoccupied states in the same TM atom. In our simulation, we take out one electron from the state to be excited, so a hole in the molecule is created and all the other orbitals (occupied and unoccupied) are allowed to shrink freely. Three simulations were performed on ZrO_2, HfO_2 and TiO_2:

i) ZrO_2: excitation from Zr 3p to 4d, 5s

ii) HfO_2: excitation from Hf 4p to 5d, 6s

iii) TiO_2: excitation from Ti 2p to 3d, 4s

Figure 4.17 gives the calculation result of excitation from Zr $3p_z$ to 4d and 5s on three different small cluster models from tetrahedral to cubic symmetry. (a) corresponds to Figure 4.8; (b) to Figure 4.9 and (c) to Figure 4.13. Relative orbital energy of 4d states and 5s are listed in the table. Similar d states splitting pattern is shown in these three models, 2 4d states in the first group and 3 4d states in the second group. The small splitting (about 1 eV) in each group is due to the polarization in Z direction since it is a $3p_z$ state excitation. This polarization effect is more dramatic in model (a) which is in tetrahedral symmetry. As a comparison, we calculate the excitation from Zr 1s core state, which has no polarization in a certain direction. Simulation result is shown in Figure 4.18, and degeneration of 4d states is found in each d state groups. Figure 4.17 shows that d state splitting is more enhancive in cubic symmetry (c) than tetrahedral symmetry (a) since the former can be treated like a double tetrahedral symmetry, and this is correct while compared with crystal field splitting diagram as presented in Figure 4.19. Eight-fold-coordination model (b) and (c) almost give the same Zr-4d* splitting even though the Zr-O bonds are quit different between the two models, this is because TM d* state splitting is determined mainly by the potential field around the TM atom. XAS studies of $M_{2,3}$ transitions in Figure 4.20 establish that relative energies of localized 4d* states, designated as a and b, and a' and b', are constant to ± 0.2 eV as function of silicate alloy composition, x, and therefore effectively independent of Si or Zr second neighbors [4.2]. These transition energies are not changed by the film morphology, amorphous or crystalline [4.3]. Deconvolution of $M_{2,3}$ spectra on ZrO_2 (x = 1) is shown in Figure 4.21 along with the ab initio calculation result as comparison. A calculated 4d states splitting of average 2.86ev is found in well agreement with XAS spectra, which is about 2.5

ev. Ab initio calculation also indicates Zr 5s anti-bonding state is 12 eV above 4d anti-bonding states, and the much smaller intensity of 5s state is due to the small transition probability from p to s.

Similar calculation were performed on HfO_2 and result of Hf $4p_z$ to 5d* and 6s* excitation is shown in Figure 4.22. An average 2.65 d states splitting is obtained and d-s splitting is 11 ev which is 1ev less than in ZrO_2. This is in good agreement with XAS spectra, however, d states splitting can't be resolved in the spectra due to life-time broadening effect [4.4].

A more complicated calculation was performed on TiO_2 in which we allow all three Ti 2p states ($2p_x$, $2p_y$, $2p_z$) mixed together and both triplet and singlet states were calculated. Result of simulation is listed in the table in Figure 4.23, however, only the singlet states are what we are interested since they are experimentally observable. The ab initio calculation shows the completely removal of degeneracy of T_{2g} (3 features) and E_g (2 features) mode. This can be seen more clearly in the comparison of Ti K1 edge on two TiO_2 models, one is in regular rutile symmetry which shows perfect degeneracy of T_{2g} and E_g groups, while the other is in distorted rutile symmetry which shows the opposite. The removal of degeneracy has also been proved by XAS spectra on $(ZrO_2)_1(TiO_2)_2$, as shown in figure 4.23. The removal of degeneracy is due to the distortion of octahedral symmetry in TiO_2 rutile (Figure 4.14). There is an elongation on axis Z and the bond angles in X-Y plane are not equal to 90°. This kind of distortion has been predicted by the Jahn-Teller theorem which states that any non-linear molecular system in a degenerate electronic state will be unstable and will undergo some kind of distortion that will lower its symmetry and split the degenerate state [4.5]. Transition probability to each 3d* states has also been calculated which indicates the

first two peaks in T_{2g} group should have much smaller intensity than the third one, and this is in excellent agreement with the spectra. However, transition probability ratio of 4th and 5th peaks in E_g group are not in good agreement with spectra which indicates that transition probabilities are sensitive to σ-bonding and 2nd neighbors to central Ti atom. In our model (Figure 4.14), each oxygen atom is terminated by the central Ti atom and 2 pseudo atoms, while in the Ti Zr alloy ($(ZrO_2)_1(TiO_2)_2$) each oxygen atom is terminated by 2 Ti atoms plus a Zr atom.

4.5.2 Inter-Atomic Excitation

We call it "Inter-Atomic excitation" because the electron is excited from one of the orbitals in oxygen to the unoccupied TM d and s states. Calculations were performed on the oxygen-centered cluster models.

X-ray absorption spectra of O 1s excitation on ZrO_2, HfO_2 and TiO_2 are presented in Fig 4.24, Fig 4.25 and Fig 4.26 along with ab inito calculation result respectively. Since more than one TM atom in each of these O-centered models, there are totally 20 4d* states in ZrO_2 (4 Zr atoms), 20 5d* states in HfO_2 (4 Hf atoms) and 15 3d* states in TiO_2 (3 Ti atoms), and some of them are overlapped as shown is the figure. Two groups of d states splitting are clearly shown in the ab initio calculation result while the small removal of degeneracy in each group is due to the boundary effect to the TM atoms (Figure. 4.15).

Excitation from oxygen 2p non-bonding state has also been calculated on the oxygen-centered model, and a band gap of 6.6 ev for ZrO_2 is predicted by ab initio calculation which in good agreement with the spectra, as shown in Figure 4.27. It also confirms that the first two features in the spectra are both Zr 4d* anti-bonding states, while Zr 5s is way above

there 4d* states (~7 eV higher). Similar features and a band gap of 7.5 eV are derived for HfO_2.

4.6 Reference

[4.1] Ralph W.G. Wyckoff, Crystal Structures, Second Edition, 1963

[4.2] Gerald Lucovsky, Bruce Rayner, Yu Zhang, Gunther Appel, Jerry Whitten, Band Offset Energies In Zirconium Silicate Si Alloys, Applied Surface Science 216 (2003) 215-222

[4.3] G. Lucovsky, G.B. Rayner Jr., D. Kang, G. Appel, R.S. Johson, Y. Zhang, D.E. Sayers, H. Ade, J.L. Whitten, Appl. Phys. Lett. 79 (2001) 1775

[4.4] G. Lucovsky, Y. Zhang, G.B. Rayner Jr., G. Appel, H. Ade, Electronic Structure of High-K Transition Metal Oxides And Their Silicate And Aluminate Alloys, J. Vac. Sci. Technol. B 20(4), Jul/Aug 2002

[4.5] H. Krebs, Fundamentals of Inorganic Crystal Chemistry, 1968

[4.6] G. Lucovsky, et al. J. Vac, Sci. Technol. **B 20**, 1739 (2002).

[4.7] G. Lucovsky, J.G. Hong, C.C. Fulton, Y. Zou, R.J. Nemanich and H. Ade, J. Vac. Sci. Technol B **22** 2132, (2004).

[4.8] G. Lucovsky and J.L. Whitten, in High-k Dielectrics, ed. by M. Houssa (Institute of Physics, Bristol, 2004).

[4.9] G. Lucovsky, et al., IEEE Transactions on Device and Materials Reliability, to be published in 2005.

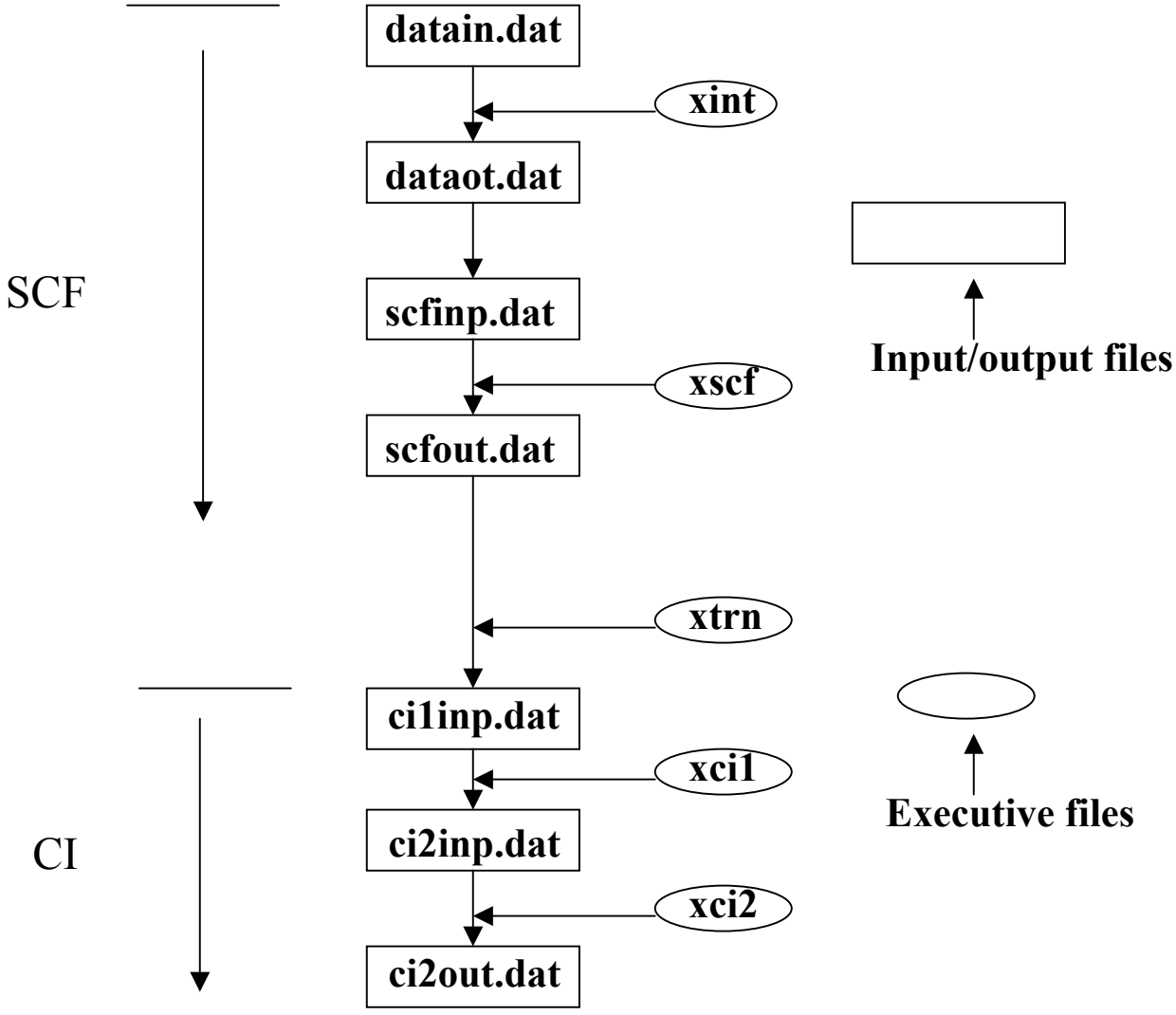

Figure 4.1 Schematic procedures of SCF and CI calculation

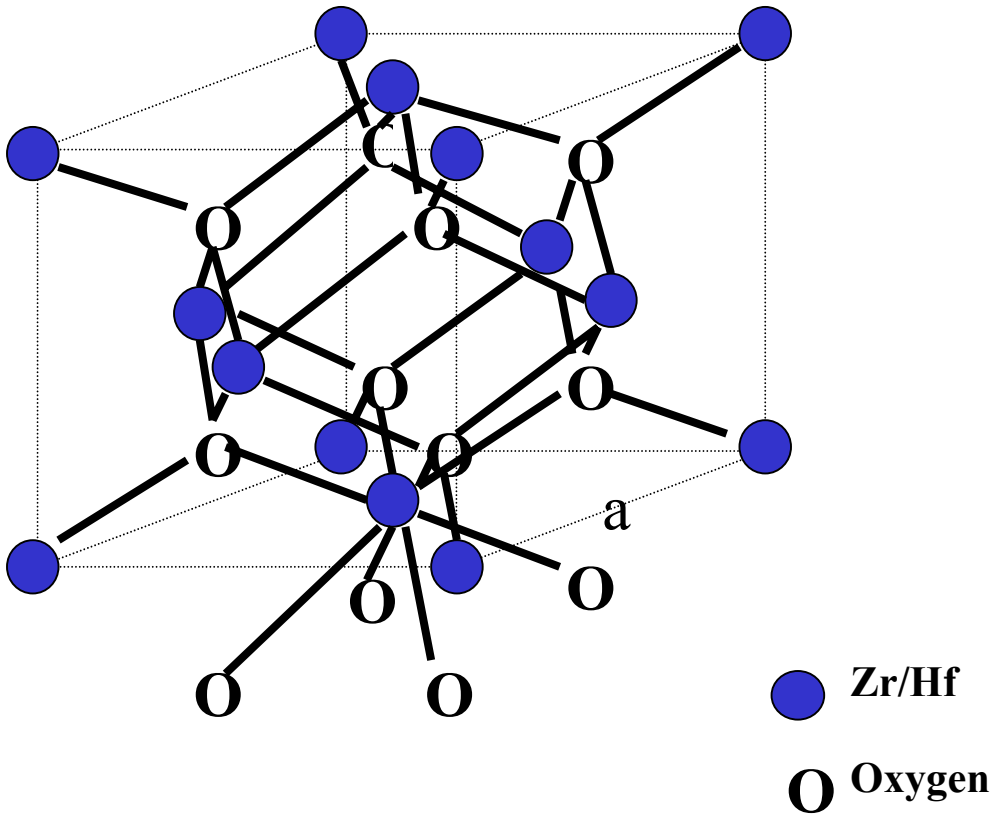

a = 5.07 Å (ZrO_2)
5.115 Å (HfO_2)

TM-O bond length: 2.2 Å

Figure 4.2 Crystal structure of ZrO_2/HfO_2 (fluorite)

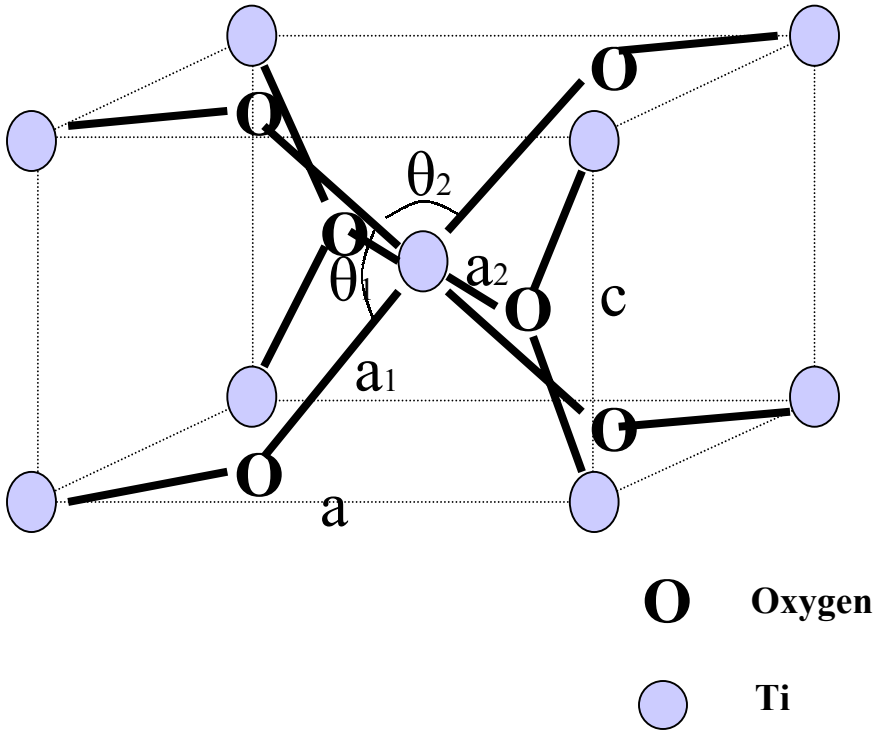

a = 4.59 Å , c = 2.96 Å

a1 = 1.95 Å , a2 = 1.98 Å

$\theta_1 = 98.9°$, $\theta_2 = 81.1°$

Figure 4.3 Crystal structure of TiO_2 (rutile)

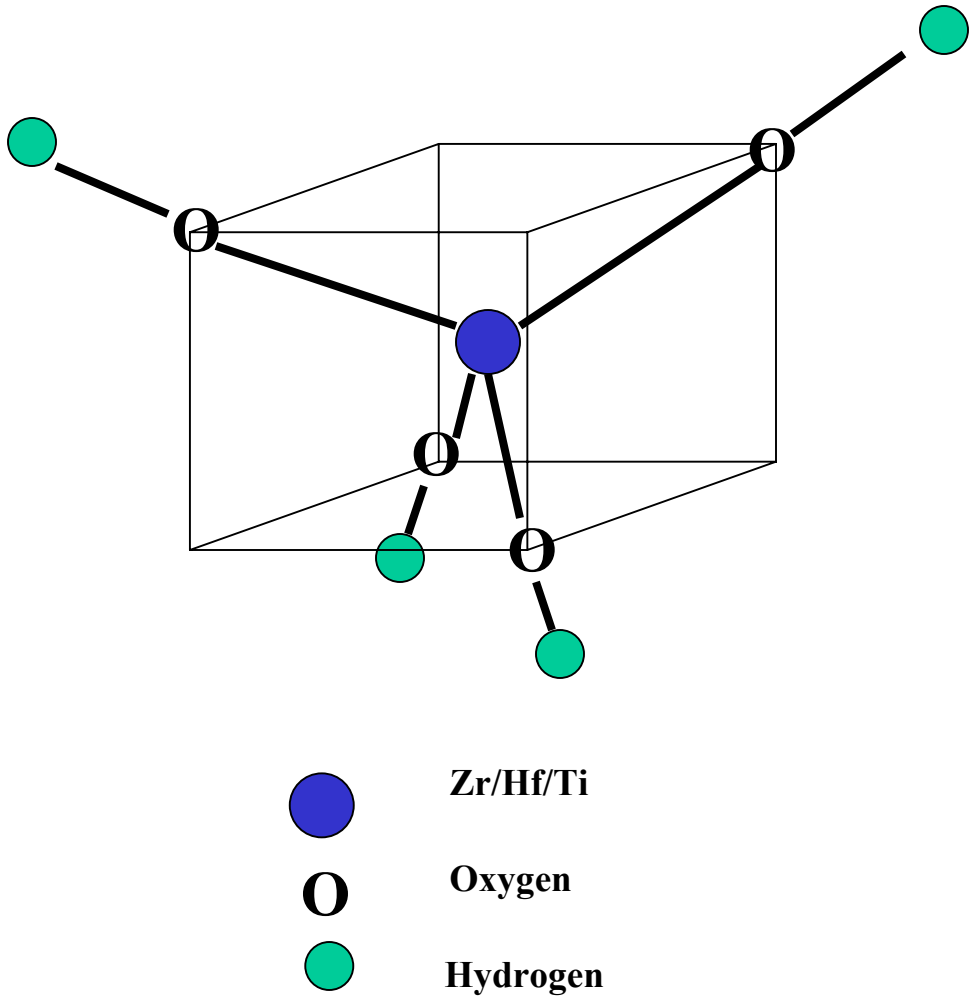

Figure 4.4 Four-fold TM-centered small cluster model $TM(OH)_4$

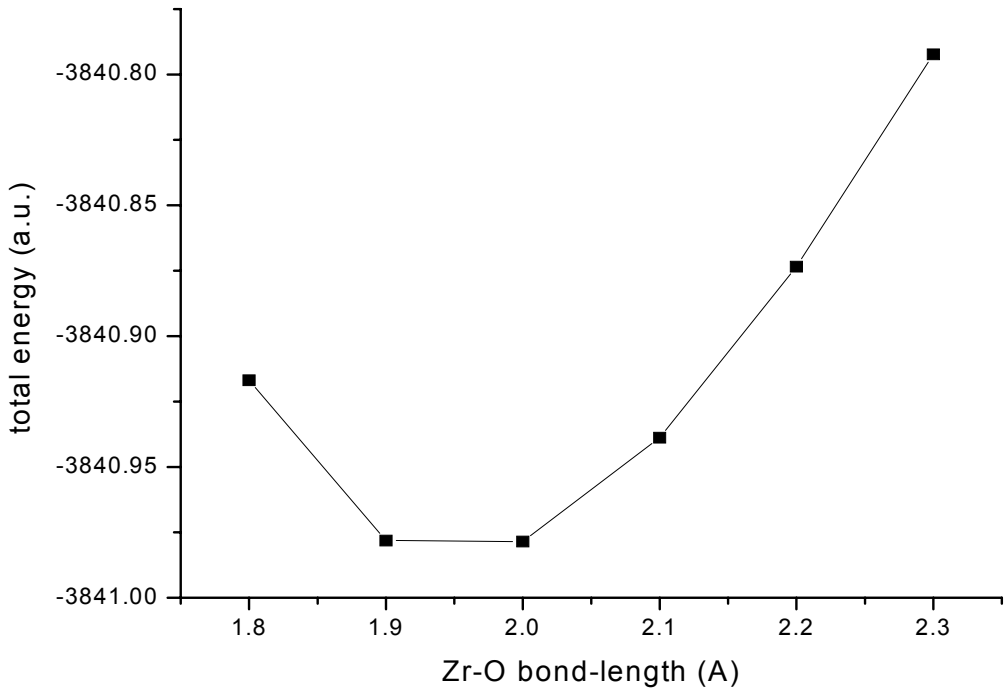

Figure 4.5 Total SCF energy vs. Zr-O bond-length

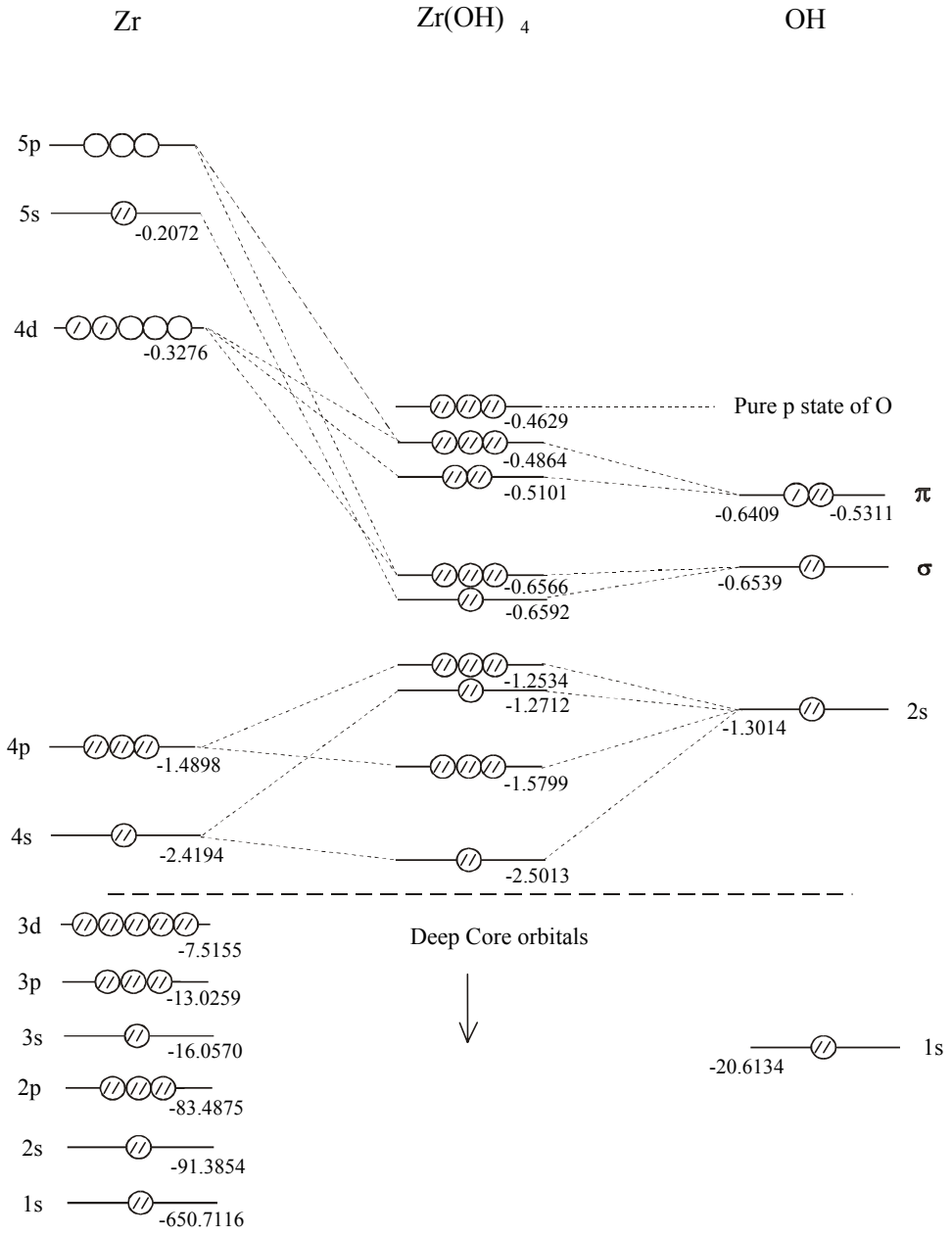

Figure 4.6 Ground states of $Zr(OH)_4$ (all energies are given in atomic units)

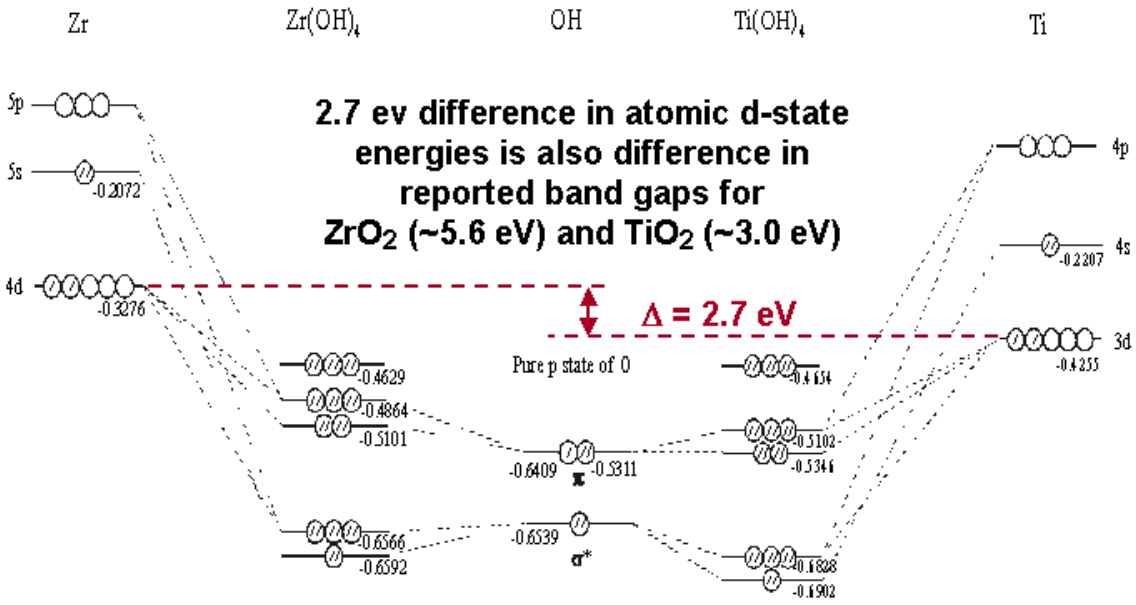

Figure 4.7 Comparison of valence band states between $Zr(OH)_4$ and $Ti(OH)_4$
(all energies are given in atomic units)

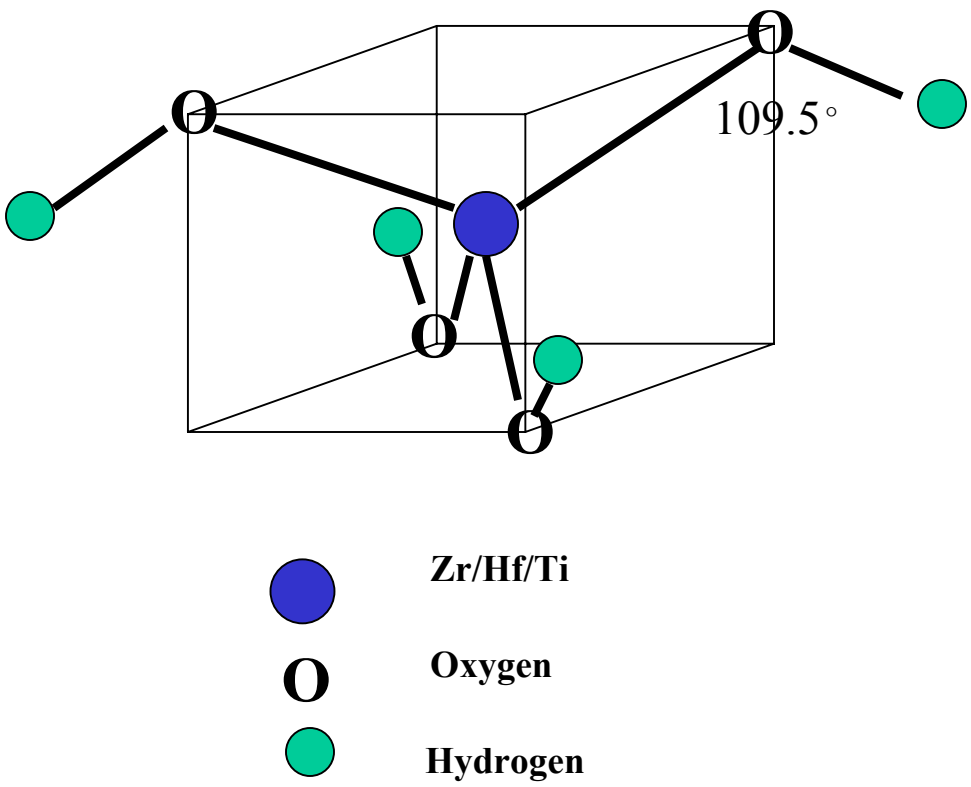

Figure 4.8 Four-fold TM-centered small cluster model $TM(OH)_4$

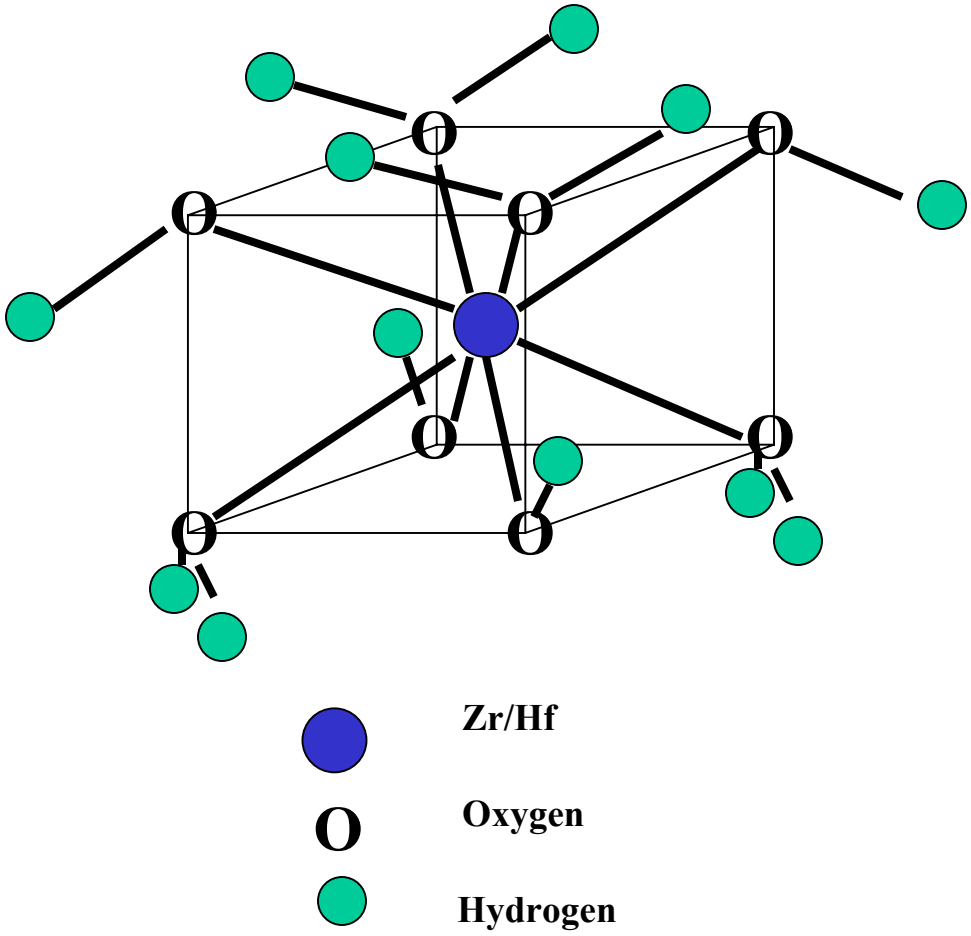

Figure 4.9 Eight-fold TM-centered small cluster model $TM(OH)_4(H_2O)_4$

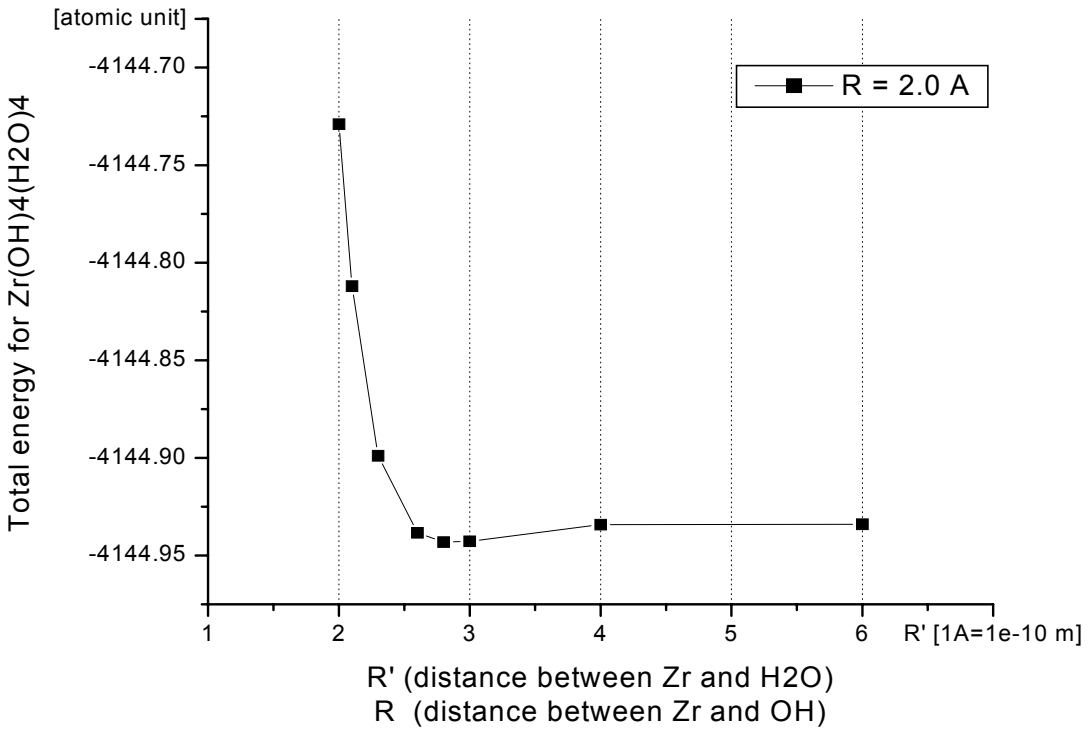

Figure 4.10 HOH polarization – total energy versus effective bond-length
Simulates effects of neighboring Si-O-Si in silicate alloys

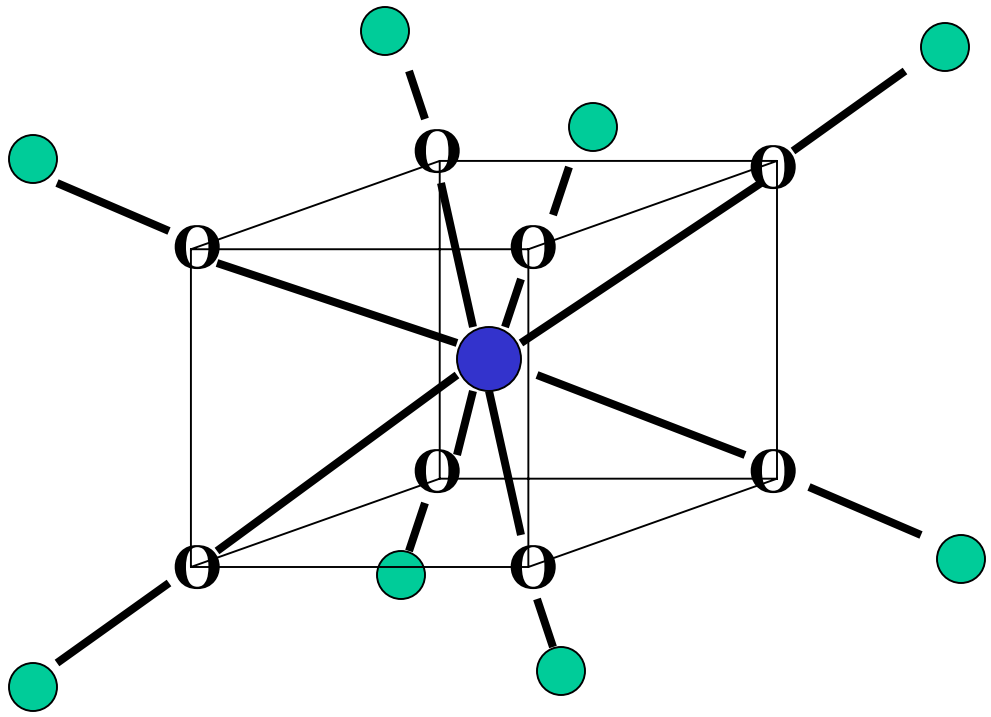

Zr/Hf

O Oxygen

Pseudo atom: Hydrogen-like atom with +1.5 charge in nuclei

Figure 4.11 Eight-fold TM-centered small cluster model $TM(OH)_8$

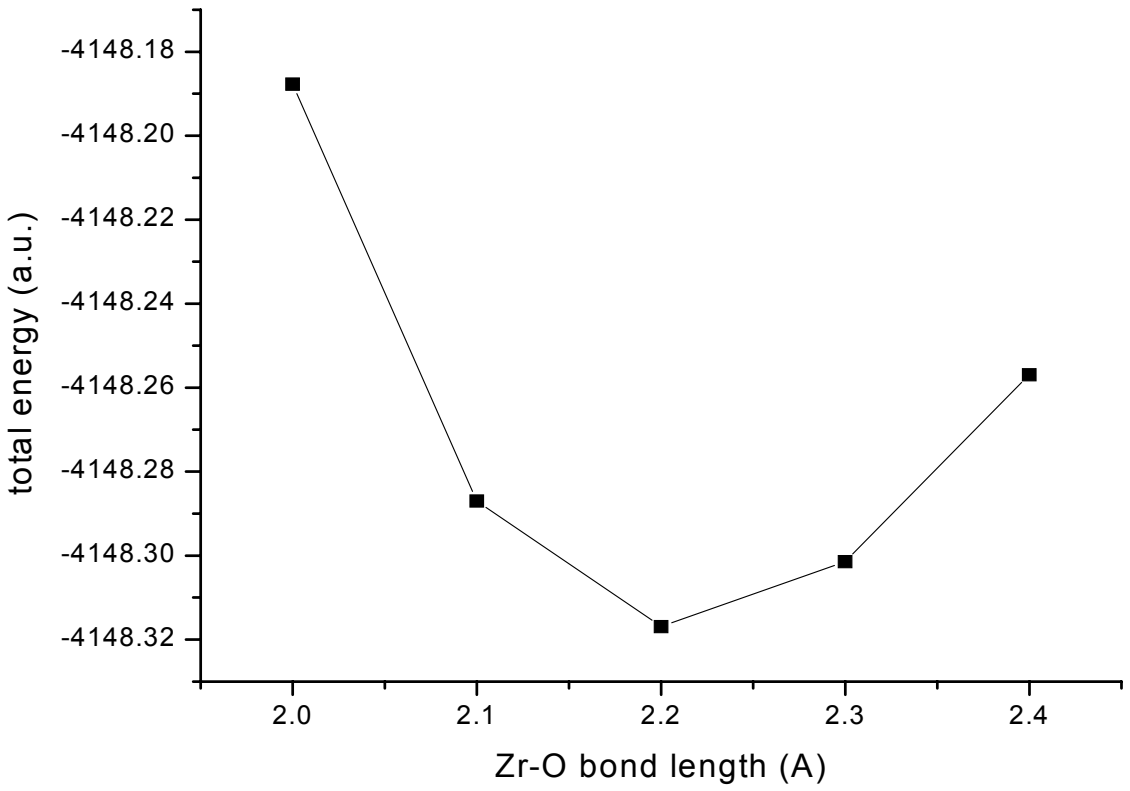

Figure 4.12 Total SCF energy vs. Zr-O bond-length in $Zr(OH)_8$

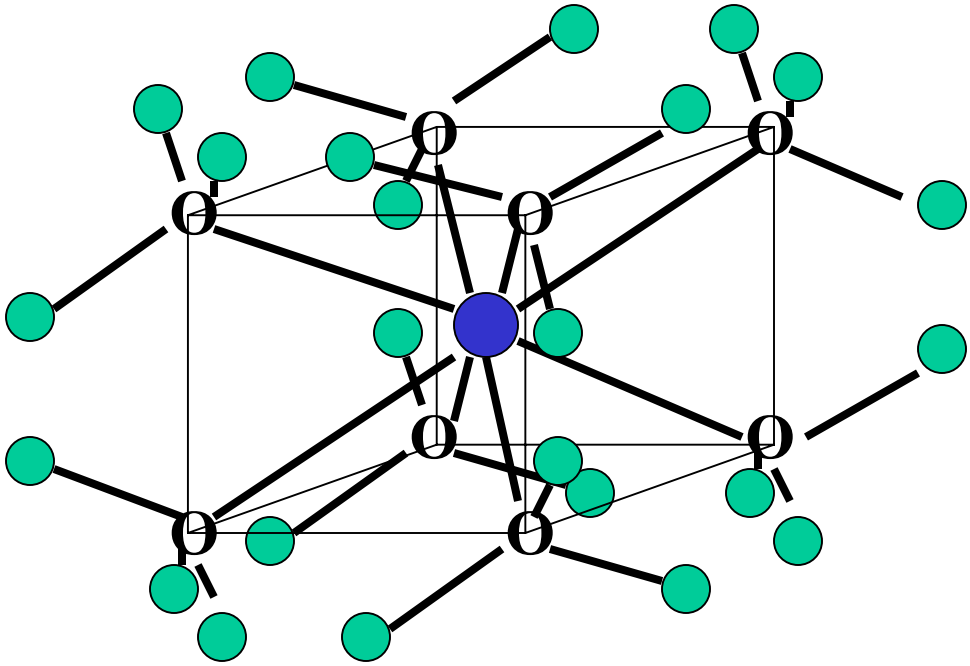

Zr/Hf

O Oxygen

Pseudo atom: Hydrogen-like atom with +0.5 charge in nuclei

Figure 4.13 Eight-fold TM-centered small cluster model $TM(OH)_8$

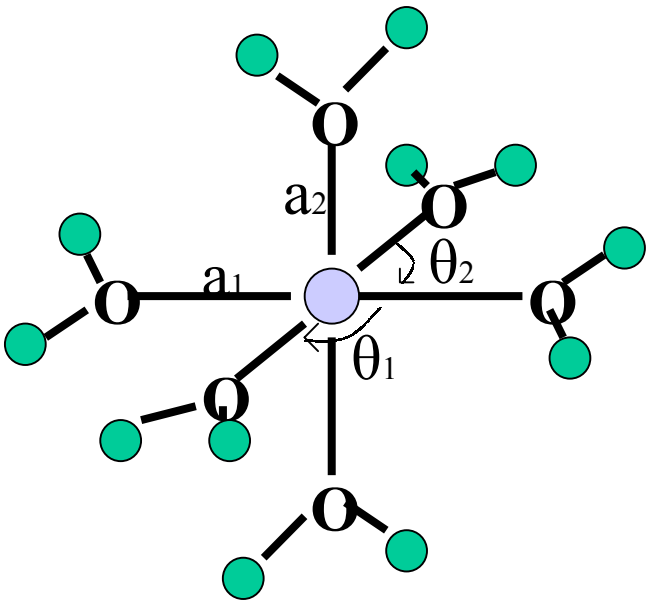

a1 = 1.95 Å , a2 = 1.98 Å

$\theta_1 = 98.9°$, $\theta_2 = 81.1°$

Ti

O **Oxygen**

Pseudo atom: Hydrogen-like atom with $+\frac{2}{3}$ charge in nuclei

Figure 4.14 Six-fold Ti-centered small cluster model $Ti(OH)_6$

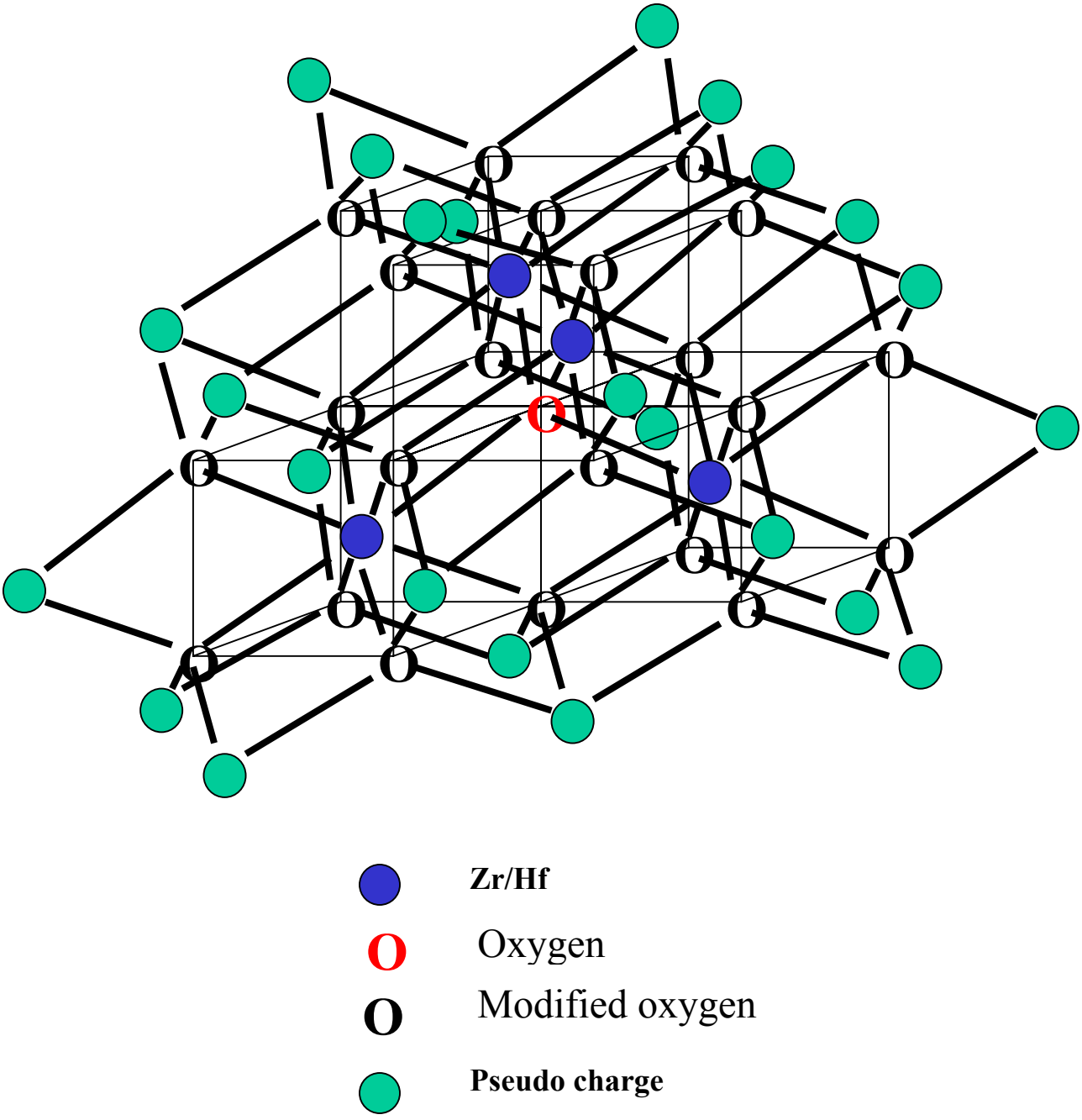

Figure 4.15 Oxygen-centered small cluster model OZr_4

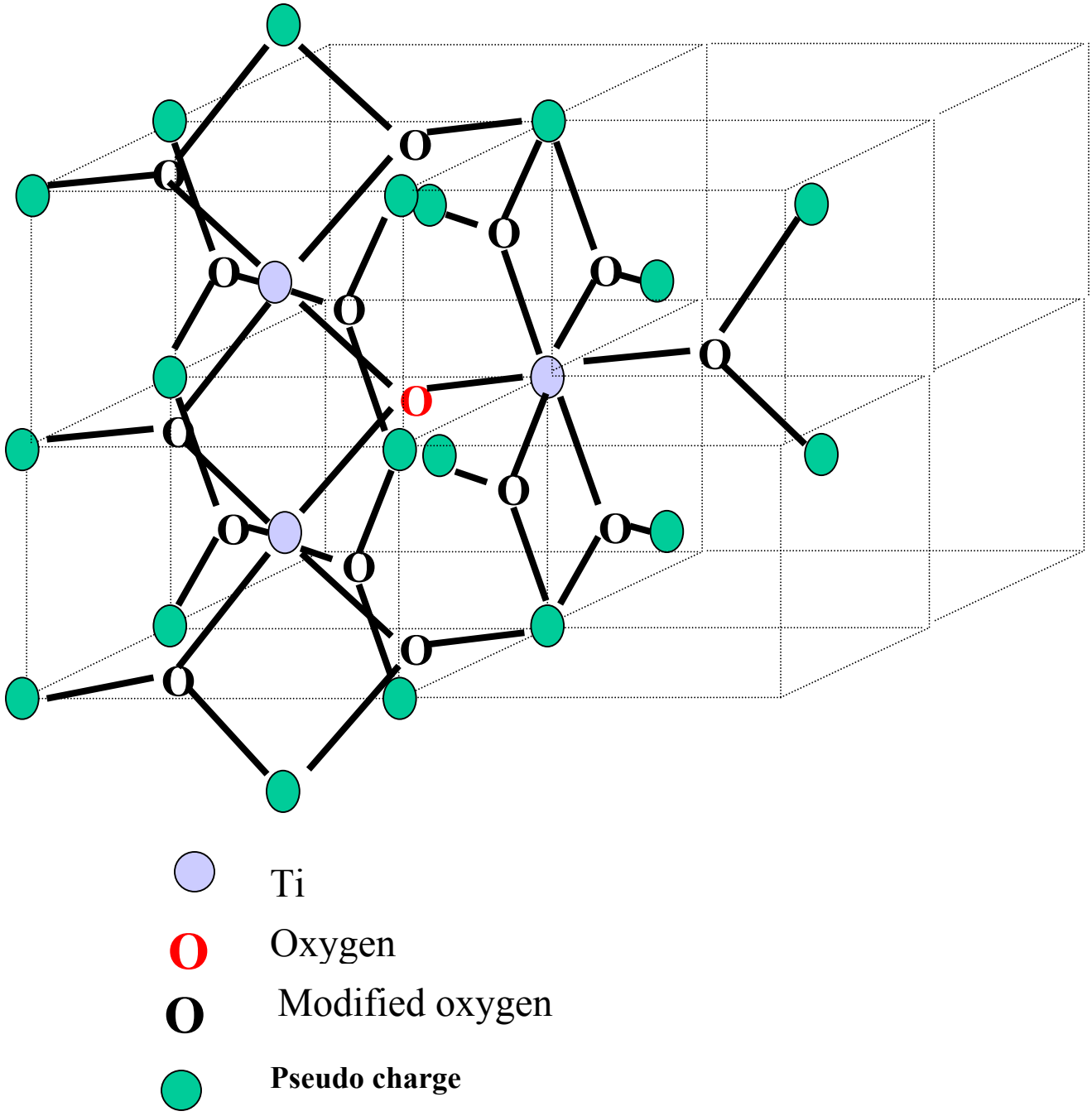

Figure 4.16 Oxygen-centered small cluster model OTi_3

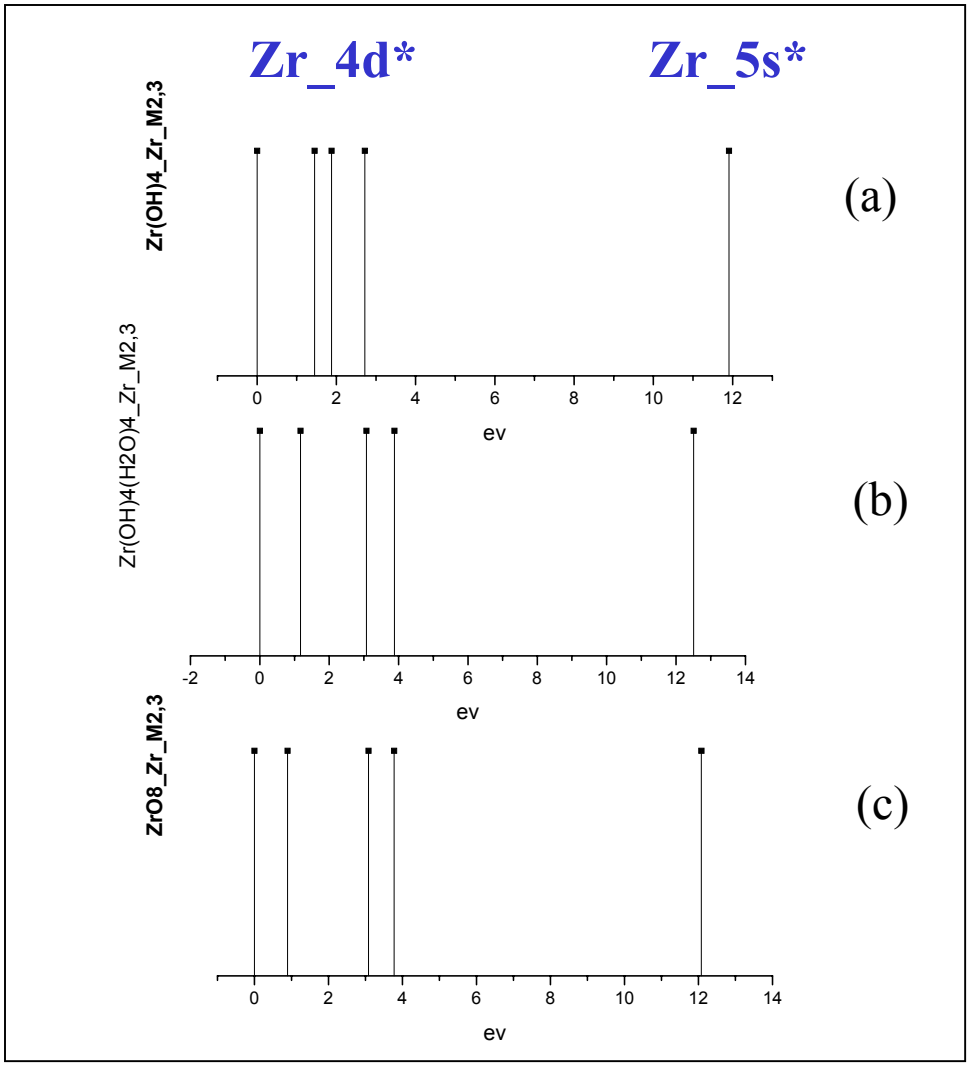

ZrO_2 / ev	$4d_1$	$4d_2$	$4d_3$	$4d_4$	$4d_5$	5s
(a)~Fig. 4.8	0.00	1.45	1.88	1.88	2.72	11.91
(b)~Fig. 4.9	0.00	1.18	3.07	3.07	3.88	12.50
(c)~Fig. 4.13	0.00	0.89	3.08	3.08	3.77	12.08

Figure 4.17 ab initio calculation of excitation from Zr 3Pz core state to Zr 4d and 5s on three different models: (a) tetrahedral; (b) cubic (4OH+4H2O); (c) cubic

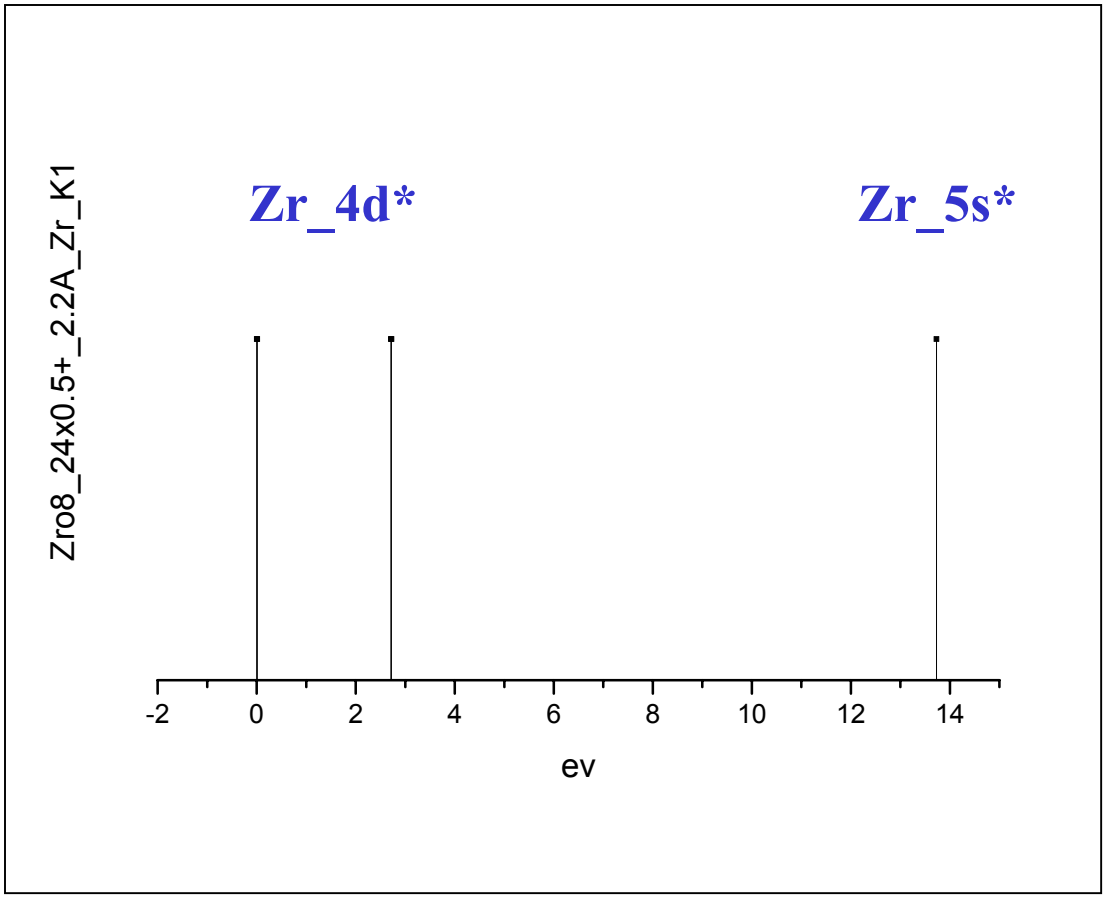

ZrO_2 / ev	$4d_1$	$4d_2$	$4d_3$	$4d_4$	$4d_5$	5s
Fig. 4.13	0.00	0.01	2.71	2.72	2.72	13.73

Figure 4.18 ab initio calculation of excitation from Zr 1s core state to Zr 4d and 5s on cubic model (Fig. 4.13)

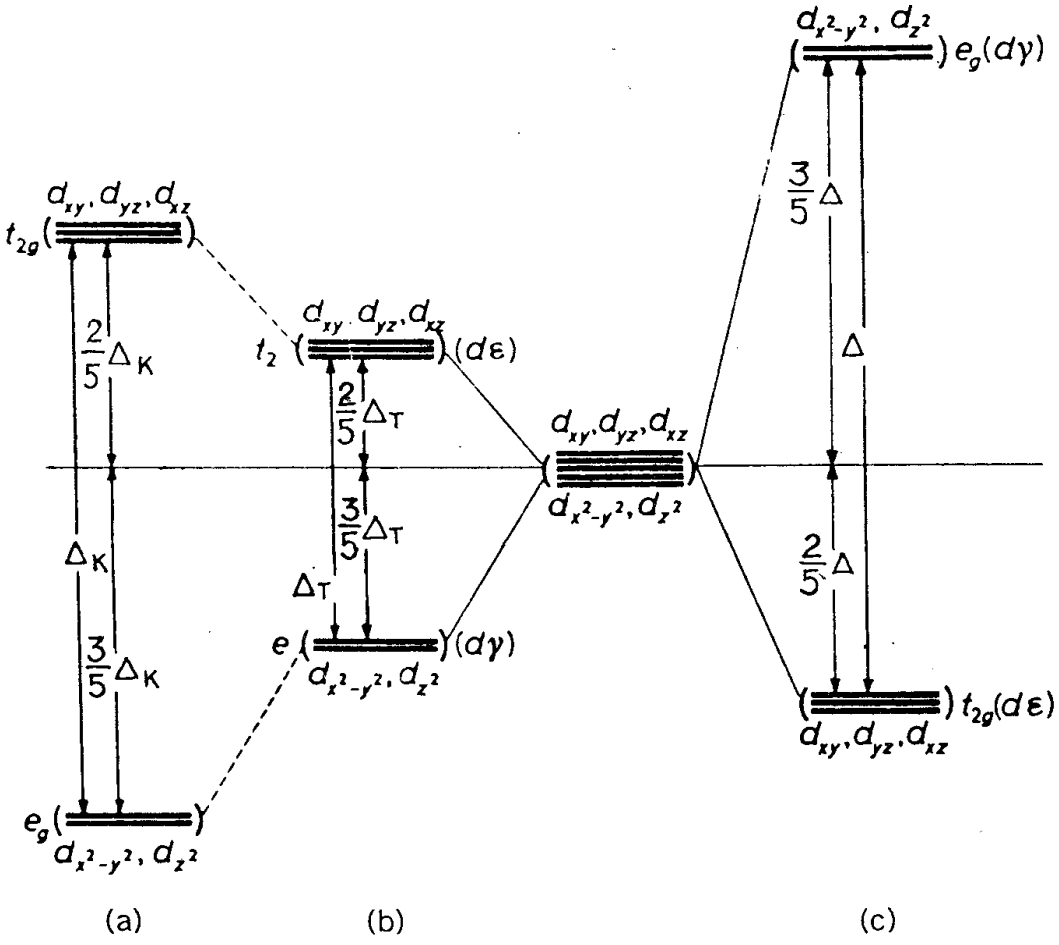

Figure 4.19 splitting of D term in cubic (a), tetrahedral (b), and octahedral (c) fields of ligands

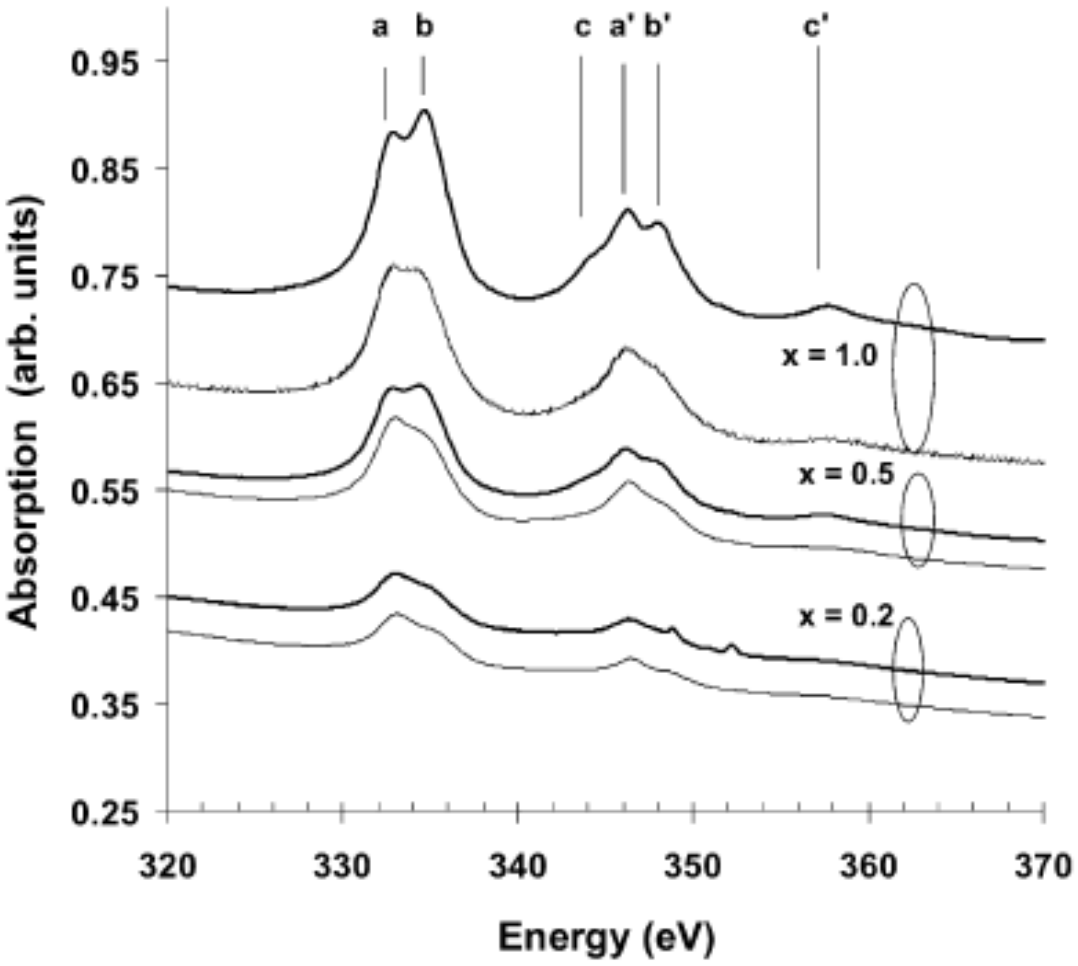

Figure 4.20 XAS $M_{2,3}$ spectra for Zr silicate alloys: a, b and c and a', b' and c' designate energy differences between the M_2 and M_3 p-states, respectively, and the respective anti-bonding Zr 4d* and 5s* states for alloys with x = 1.0, 0.5 and 0.2. [4.2]

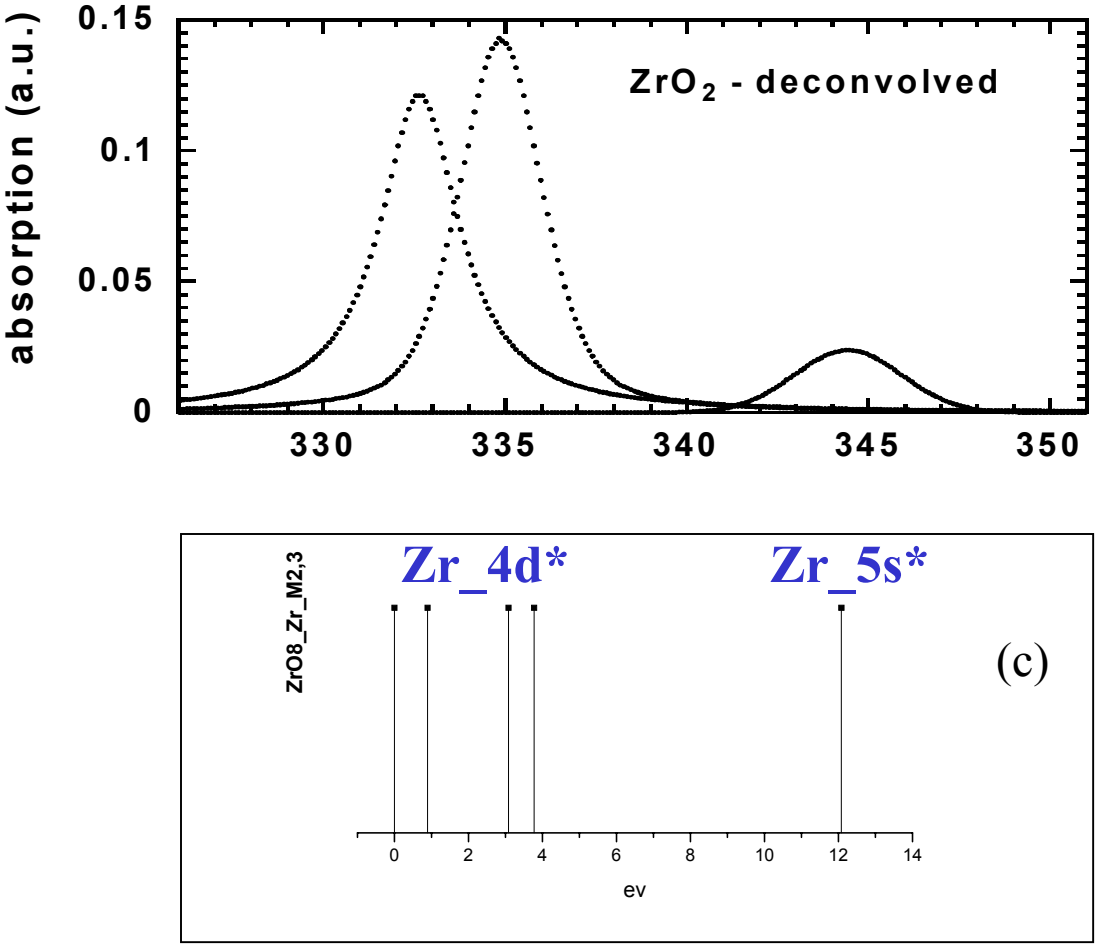

Figure 4.21 comparison of XAS Zr $M_{2,3}$ on ZrO_2 and ab initio calculation on cubic model (c)

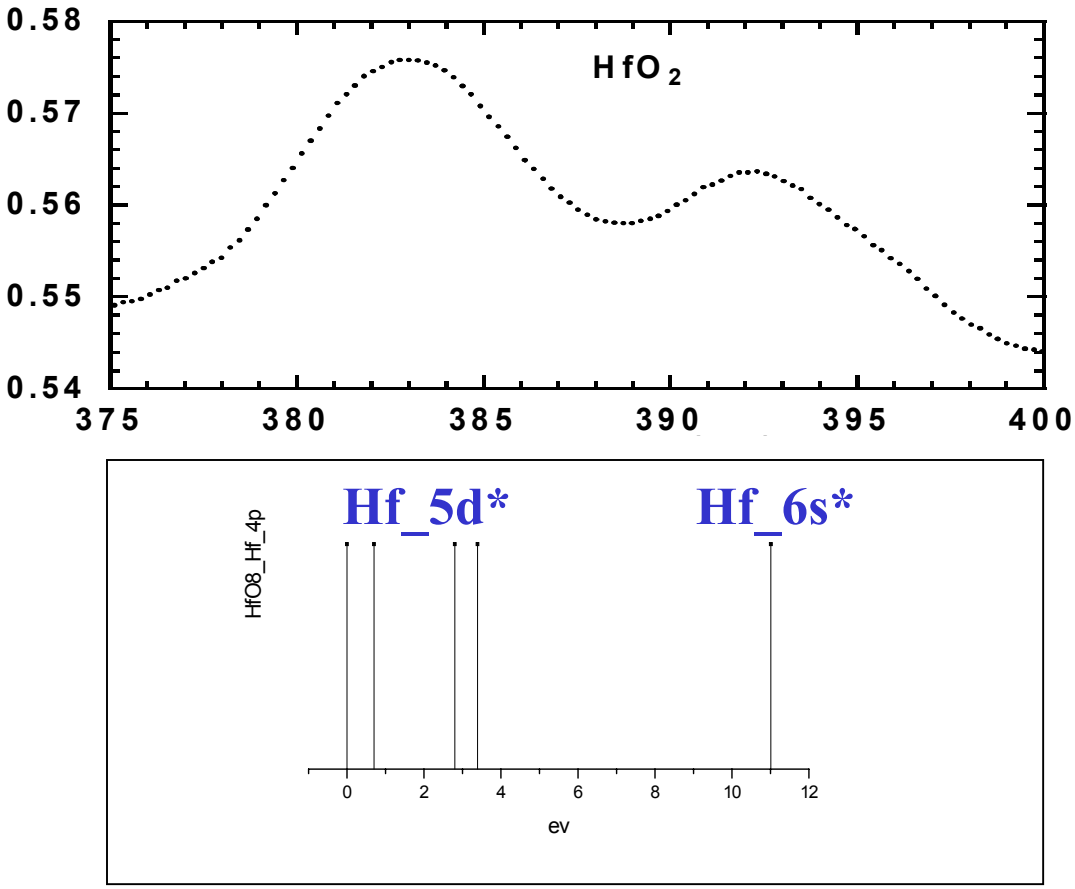

HfO_2 / ev	$5d_1$	$5d_2$	$5d_3$	$5d_4$	$5d_5$	6s
Fig. 4.13	0.00	0.70	2.80	2.80	3.39	11.01

Figure 4.22 comparison of XAS Hf 4p on HfO_2 [4.6, 4.7, 4.8, 4.9] and ab initio calculation on cubic model (c)

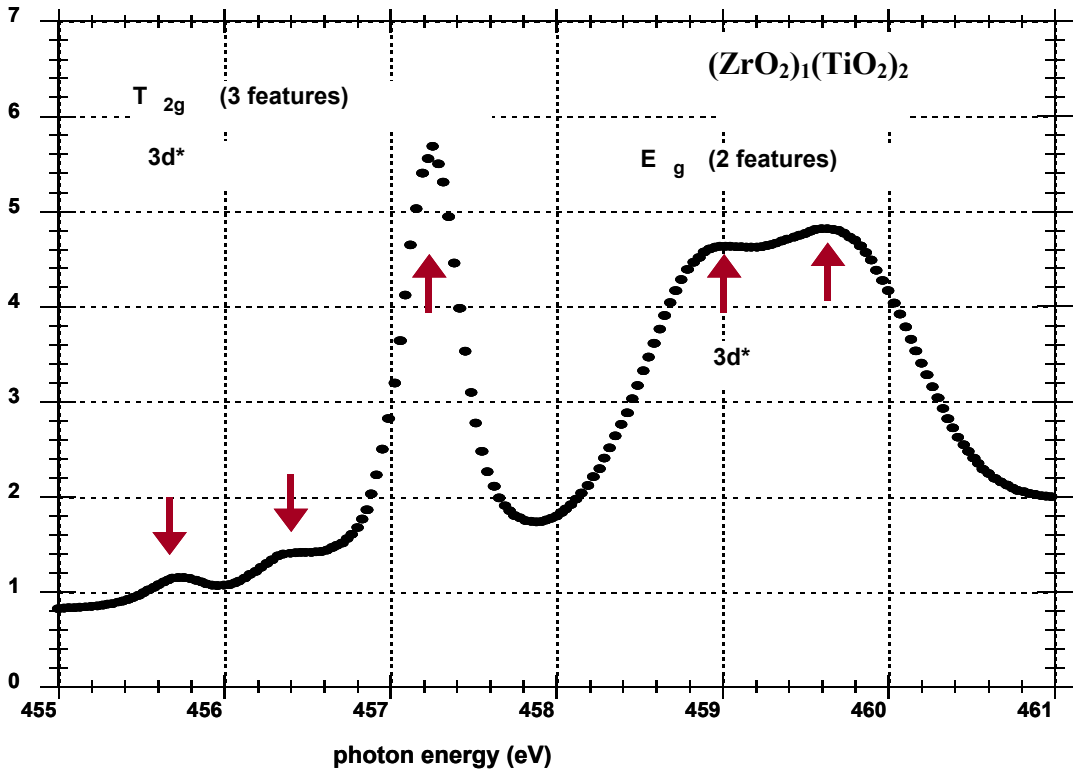

Triplet state (ev)		Singlet state (ev)	Transition Probability
0.00	3d1	0.00	1
0.75	3d2	0.58	0.9
1.78	3d3	1.12	21
3.04	3d4	3.16	1
4.33	3d5	4.86	121

Figure 4.23 comparison of XAS Ti 2p on $(ZrO_2)_1(TiO_2)_2$ [4.6, 4.7, 4.8, 4.9] and ab initio calculation on distorted rutile model (Figure 4.14)

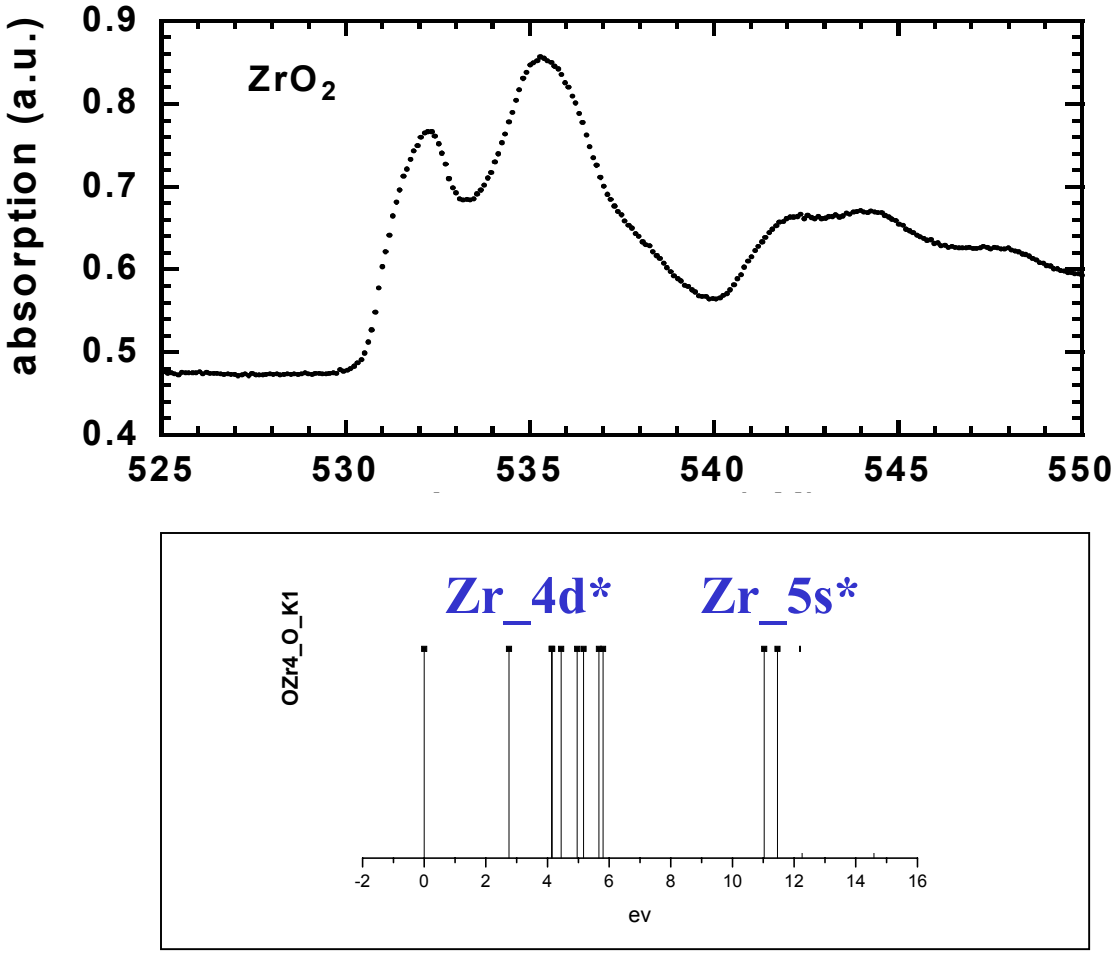

Figure 4.24 comparison of XAS O K_1 on ZrO_2 [4.6, 4.7, 4.8, 4.9] and ab initio calculation on oxygen-centered model (Figure 4.15)

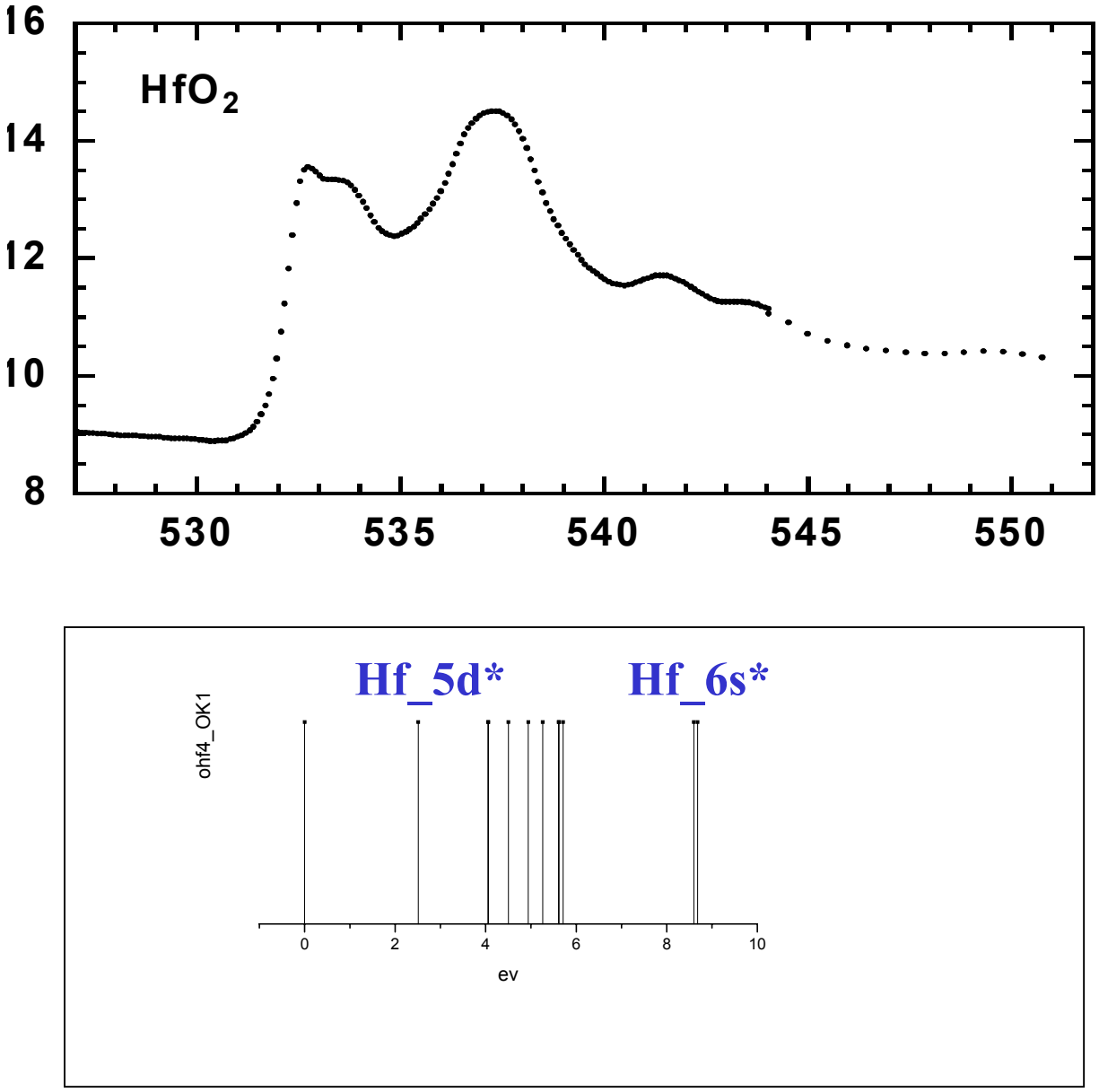

Figure 4.25 comparison of XAS O K_1 on HfO_2 [4.6, 4.7, 4.8, 4.9] and ab initio calculation on oxygen-centered model (Figure 4.15)

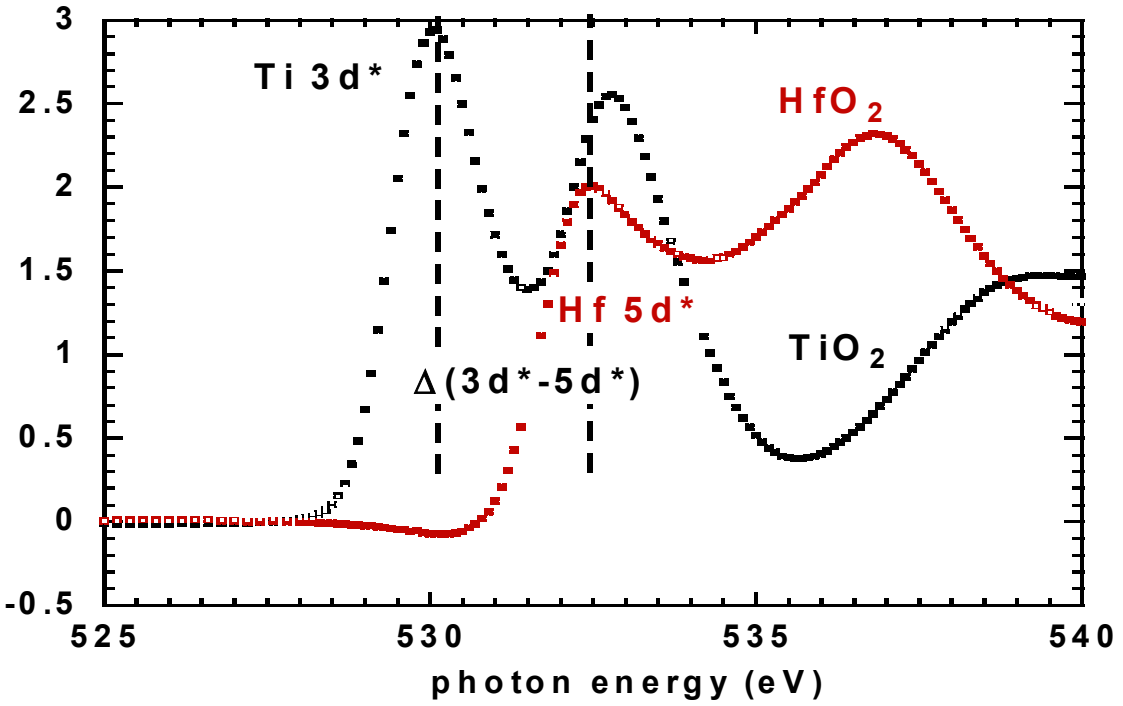

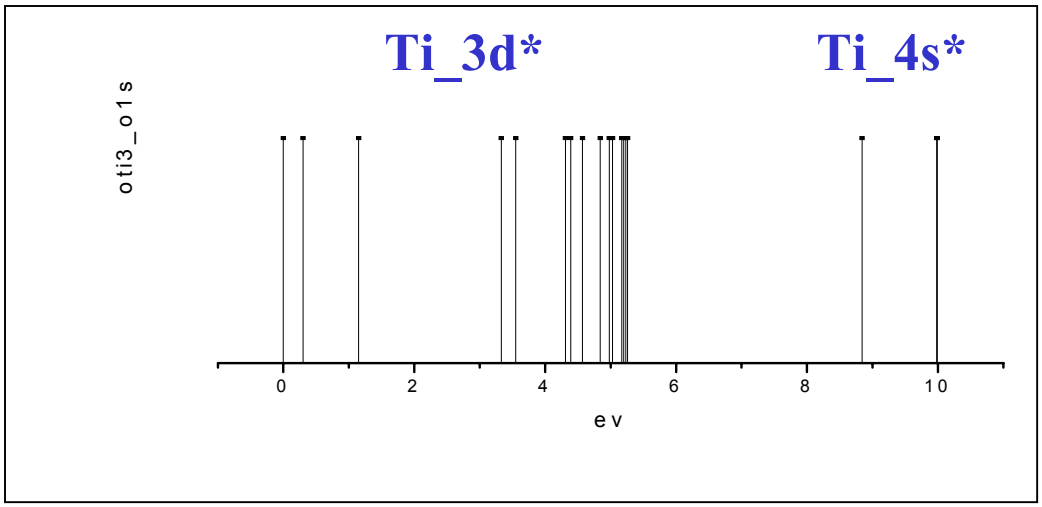

Figure 4.26 comparison of XAS O K_1 on TiO_2 [4.6, 4.7, 4.8, 4.9] and ab initio calculation on oxygen-centered model (Figure 4.16)

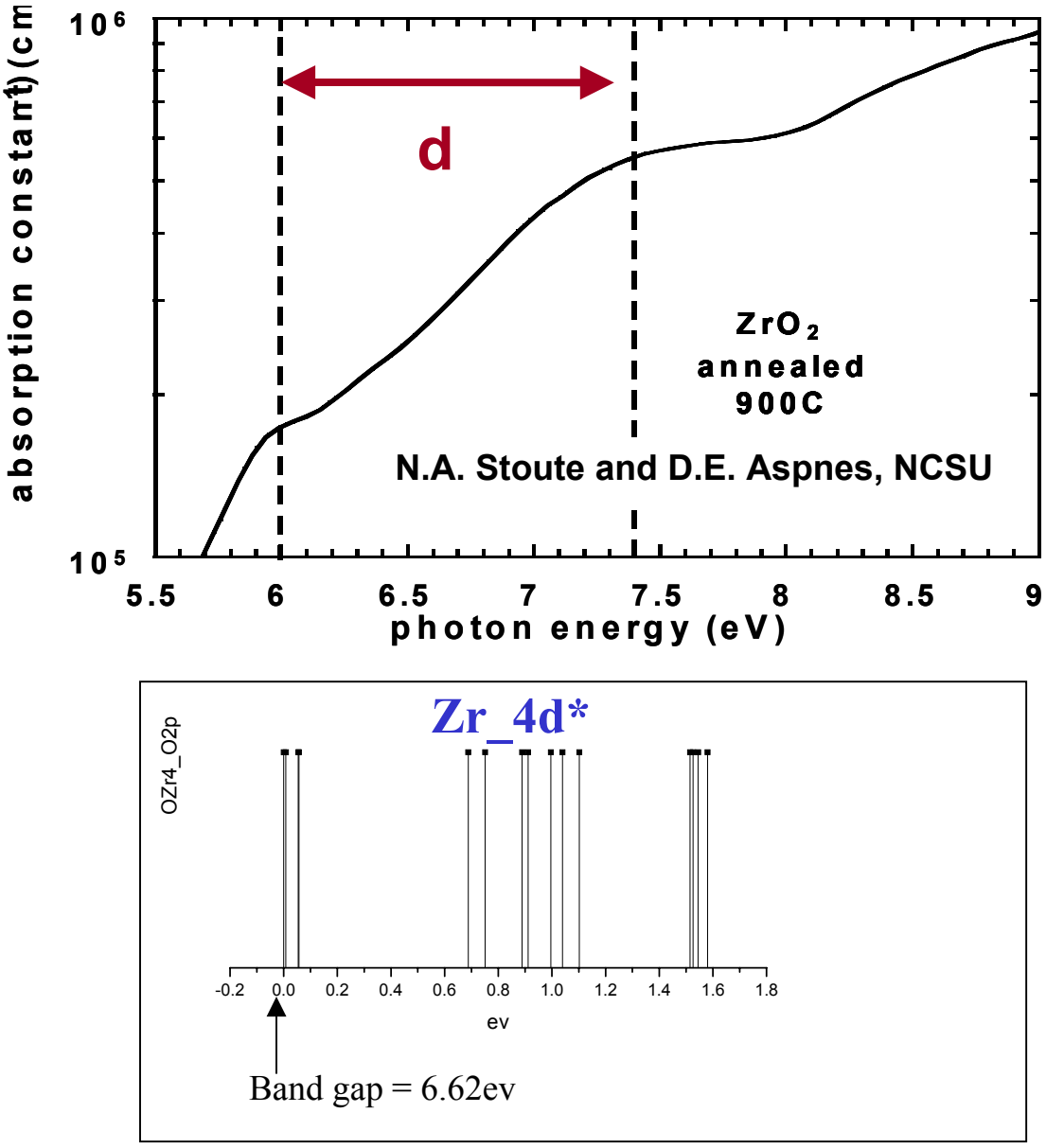

Figure 4.27 comparison of XAS O 2p on ZrO_2 and ab initio calculation on oxygen-centered model (Figure 4.15)

Chapter 5. Summary And Conclusion

The objective of this theoretical study is to provide an understanding of the electronic structure of high-k elemental and complex oxides. The calculations are many-body ab initio calculations which are done at the Hartree-Fock self consistent field (SCF) level and also utilize Correlation Interaction (CI) refinements.

Two different cluster models are used, one centered on the transition metal, and one on the oxygen atoms. i) TM-centered models use full atomic basis sets for the central TM atom, and its immediate oxygen neighbors, reflecting the 6-fold coordination of Ti in TiO_2, and the 8-fold coordination of Zr and Hf in ZrO_2 and HfO_2. More distant neighbors are represented by pseudo atoms with charges used to make the whole cluster neutral and has zero dipole moment. ii) O-centered models use full atomic basis set for the central oxygen atom, and "simplified" atomic basis for its first neighbors, reflecting the 3-fold coordination of O in TiO_2, and4-fold coordination of O in ZrO_2 and HfO_2. "modified" oxygen atoms that are determined in a self-consistent manner are used as the second neighbor to the central oxygen. At the boundary, charges are also used to balance the whole cluster.

The ground state calculations of transition metal-oxygen bond-lengths, valence band structure and core levels (not including spin-orbit splittings) are in good agreement with experiment. Top of valence band states of TM oxides and silicates have been determined to be non-bonding Oxygen 2p states, and the lowest conduction bands from localized TM d-states.

Final state configurations have also been calculated. Using the cluster models centered on transition metal atoms, these calculations have focused on the Zr $M_{2,3}$, Hf $N_{2,3}$ and Ti $L_{2,3}$ edges, and Ti, Zr and Hf K_1 edges as well. Relative energies of the Ti 3d*, Zr 4d*

and Hf 5d* state doublets, and Ti 4s*, Zr 5s*, and Hf 6s* state features have been identified in the respective transition metal oxides. XAS measurements [5.1] confirm the localization of conduction band d* states, and their insensitivity to second neighbor atoms. Using the cluster models centered on the oxygen atoms, the calculations have focused on the O K_1 edges, and the band edge transitions. The final states for these transitions show the mixing of O 2p* states with the respective transition metal d* and s* states, but with different relative energies.

In general, the agreement between all of these calculations and the spectroscopy studies has been very good, and the small cluster models works very well in the simulations of TM and O core excitation since the final d* states are localized on transition metal and not sensitive to its second neighbors therefore allow us to terminate the cluster with pseudo boundary. Ab initio calculations identified important correlations between atomic transition metal d and s state energies, band gaps, and conduction band offset energies that provide important guidelines for narrowing the scale of transition metals that have alignments with the Si conduction and valence bands that can provide adequate tunneling barriers [5.1, 5.2, 5.3, 5.4, 5.5].

Reference

[5.1] Gerald Lucovsky, Bruce Rayner, Yu Zhang, Gunther Appel, Jerry Whitten, Applied Surface Science 216 (2003) 215-222

[5.2] G. Lucovsky, Y. Zhang, G. B. Rayner, Jr., G. Appel, H. Ade and J. L. Whitten, J. Vac. Sci. Technol. B 20(4), 1739-1747, Jul/Aug 2002

[5.3] G. B. Rayner, Jr., D. Kang, Y. Zhang, and G. Lucovsky, J. Vac. Sci. Technol. B 20(4), 1748-1758, Jul/Aug 2002

[5.4] G. Lucovsky, J. L. Whitten, Y. Zhang, Solid-State Electronics 46 (2002) 1687-1697

[5.5] G. Lucovsky, Bruce Rayner, Yu Zhang, Charles C. Futon. Robert J. Nemanich, Guenther Appel, Harald Ade, Jerry L. Whitten, Applied Surface Science 212-213 (2003) 563-569

Appendix A

Reference Orbitals (GTO) For Zr, Hf, Ti, O, H Atoms

(1) Zr (s, p, d)

```
  1   4   1   4   0   0     s1
.50459795E+04  .16972038E+05  .72179137E+05  .47742451E+06   (Exponent)
0.054915431    0.014686324    0.003030831    0.000399530     (Coefficient)
  2   1   1   1   0   0     s2
.50459795E+04
1.0
  3   1   1   1   0   0     s3
.17286244E+04
1.0
  4   1   1   1   0   0     s4
.66301410E+03
1.0
  5   1   1   1   0   0     s5
.27452888E+03
1.0
  6   1   1   1   0   0     s6
.11895280E+03
1.0
  7   1   1   1   0   0     s7
.44331005E+02
1.0
  8   1   1   1   0   0     s8
.19458012E+02
1.0
  9   1   1   1   0   0     s9
.64365559E+01
1.0
 10   1   1   1   0   0     s10
.31369765E+01
1.0
 11   1   1   1   0   0     s11
.16769577E+01
1.0
 12   1   1   1   0   0     s12
.75794368E+00
1.0
 13   1   1   1   0   0     s13
.35251601E+00
1.0
 14   1   1   1   0   0     s14
.72983731E-01
1.0
 15   1   1   1   0   0     s15
.28630798E-01
1.0
```

```
 16   4   2   4   0   0     p1
.12497249E+03  .32797906E+03  .10133501E+04  .42711765E+04
0.272403287    0.093783339    0.019829951    0.002413984
 17   1   2   1   0   0     p2
.12497249E+03
0.272403287
 18   1   2   1   0   0     p2
.52676385E+02
1.0
 19   1   2   1   0   0     p3
.23613474E+02
1.0
 20   1   2   1   0   0     p4
.98279363E+01
1.0
 21   1   2   1   0   0     p5
.42470841E+01
1.0
 22   1   2   1   0   0     p6
.16539778E+01
1.0
 23   1   2   1   0   0     p7
.71245766E+00
1.0
 24   1   2   1   0   0     p8
.27571726E+00
1.0
 42   1   2   1   0   0     p9
0.08
1.0



 25   4   4   4   0   0     d1
.65072003E+01  .15823177E+02  .42117280E+02  .14405409E+03
0.445852933    0.357085937    0.147093209    0.025712189
 26   1   4   1   0   0     d2
.27336987E+01
1.0
 27   1   4   1   0   0     d3
.97846411E+00
1.0
 28   1   4   1   0   0     d4
.35016420E+00
1.0
 29   1   4   1   0   0     d5
.11671223E+00
1.0
```

(2) Hf (s, p, d, f)

```
 1  11   1   2   0   0     s1   ( 1s+ )
.34987624E+03  .74086305E+03  .16166312E+04  .37443842E+04  .94053341E+04          (Exponent)
.26014132E+05  .79687141E+05  .26295675E+06  .92603505E+06  .37381476E+07
.22818066E+08
9.6549476E-02  2.8077264E-01  3.2504085E-01  2.2754190E-01  1.1861788E-01          (Coefficient)
5.2024476E-02  2.0393195E-02  7.6427422E-03  2.9372890E-03  1.1865563E-03
4.1590770E-04
 2   5   1   2   0   0     s2   ( 2s+ )
.19411443E+02  .39435844E+02  .81289754E+02  .16805174E+03  .34987624E+03
4.2489421E-03  7.9056905E-02  4.8948651E-01  5.2162938E-01  5.3034683E-02
 3   5   1   2   0   0     s3   ( 3s+ )
.22110692E+01  .45211968E+01  .93316112E+01  .19411443E+02  .39435844E+02
-7.7827460E-03  1.3040553E-02  1.3900305E-01  8.6030386E-01  4.1541494E-01
 17   5   1   2   0   0     s   ( 4s+ )
.51870059E+00  .11017947E+01  .22110692E+01  .45211968E+01  .93316112E+01
4.7312121E-03 -1.4259316E-02 -2.0107504E-01 -9.9443478E-01 -3.0616487E-01
 25   6   1   2   0   0     s   ( 5s+ )
.22527601E+00  .51870059E+00  .11017947E+01  .22110692E+01  .45211968E+01
.93316112E+01
-6.1329716E-02 -6.2816024E-01 -7.4585492E-01  2.3697487E-01  8.5023879E-01
 2.0567626E-01
 4   6   1   2   0   0     s4   ( 6s+ )
.26014132E+05  .79687141E+05  .26295675E+06  .92603505E+06  .37381476E+07
.22818066E+08
-5.2835551E-04  -2.0058365E-4  -7.3709370E-5  -2.7863115E-5  -1.1136466E-5
-3.8693056E-6
 5   4   1   3   0   0     s5
.74086305E+03  .16166312E+04  .37443842E+04  .94053341E+04
-5.1856689E-03 -4.6073119E-03 -2.6943328E-03 -1.2641872E-03
 6   3   1   3   0   0     s6
.81289754E+02  .16805174E+03  .34987624E+03
4.2419772E-02  2.7345898E-02  2.9252723E-03
 7   2   1   2   0   0     s7
.19411443E+02  .39435844E+02
-1.4678417E-01 -4.8319174E-02
 8   3   1   3   0   0     s8
.22110692E+01  .45211968E+01  .93316112E+01
6.6241181E-02  2.6475061E-01  5.6351000E-02
 9   2   1   2   0   0     s9
.51870059E+00  .11017947E+01
-4.4048182E-01 -2.6991874E-01
 10   4   1   3   0   0     s10
.27910104E-01  .51021537E-01  .84931703E-01  .22527601E+00
2.8727648E-01  2.6940559E-01  6.1226474E-01  1.7901218E-02




 16   1   1   0   0   1     (4f core)
 2.2
-10.87429055
```

```
 18  10   2   2   0   0      p1   ( 2p+ )
.81289754E+02  .16805174E+03  .34987624E+03  .74086305E+03  .16166312E+04
.37443842E+04  .94053341E+04  .26014132E+05  .79687141E+05  .26295675E+06
2.4828033E-01  3.9367389E-01  2.8588350E-01  1.3464438E-01  4.9925468E-02
1.5666702E-02  4.1888446E-03  9.7609513E-04  2.0188796E-04  3.7253545E-05
 19   6   2   2   0   0      p1   ( 3p+ )
.93316112E+01  .19411443E+02  .39435844E+02  .81289754E+02  .16805174E+03
.34987624E+03
9.7209440E-02  5.0773130E-01  5.0208623E-01 -2.3736468E-02 -2.3725688E-01
-1.6687392E-01
 20   5   2   2   0   0      p1   ( 4p+ )
.11017947E+01  .22110692E+01  .45211968E+01  .93316112E+01  .19411443E+02
1.2885053E-02  1.8095920E-01  6.4379627E-01  4.2647634E-01 -3.7148494E-01
 21   3   2   2   0   0      p1   ( 5p+ )
.22527601E+00  .51870059E+00  .11017947E+01
-1.6048639E-01 -5.2096337E-01 -4.8322257E-01
 22   3   2   2   0   0      p2   ( 5p+ )
.22110692E+01  .45211968E+01  .93316112E+01
9.2725814E-03  3.7097726E-01  2.2240280E-01
 23   3   2   2   0   0      p3   ( 5p+ )
.19411443E+02  .39435844E+02  .81289754E+02
-1.3800211E-01 -1.4946296E-01 -4.2012083E-03
 24   5   2   2   0   0      p4   ( 5p+ )
.16805174E+03  .34987624E+03  .74086305E+03  .16166312E+04  .37443842E+04
4.1538275E-02  2.9482795E-02  1.2798138E-02  4.5893798E-03  1.3914734E-03


 11   4   4   2   0   0      d1   ( 3D+ )
.19411443E+02  .39435844E+02  .81289754E+02  .16805174E+03
2.6801722E-01  4.1850722E-01  2.9444651E-01  1.2502868E-01
 12   3   4   2   0   0      d2   ( 4D+ )
.22110692E+01  .45211968E+01  .93316112E+01
-1.9379125E-01 -4.6262061E-01 -4.1972378E-01
 13   5   4   2   0   0      d3   ( 5D+ )
.39435844E+02  .81289754E+02  .16805174E+03  .34987624E+03  .74086305E+03
4.1754359E-02  3.1371829E-02  1.3466006E-02  4.0142132E-03  1.0487244E-03
 14   3   4   3   0   0      d4   ( 5D+ )
.45211968E+01  .93316112E+01  .19411443E+02
-1.1084234E-01 -1.0496048E-01 -1.1947772E-02
 15   5   4   3   0   0      d5   ( 5D+ )
.84931703E-01  .22527601E+00  .51870059E+00  .11017947E+01  .22110692E+01
2.9073792E-01  4.0529320E-01  3.5029964E-01  1.8669130E-01  1.1071828E-02
```

(3) H (s)

```
 21   4   1   2   0   0      (H s1)
   .32584785    1.14780265     4.9597738     32.393455
  2.47509199    1.0           .22825627      .03153557
   .32584785    1.51716735
  2.47509199    1.221871
 22   1   1   1   0   0      (H s2)
   .10297
  1.0
```

(4) Ti (s, p, d)

```
 1   6 01   6   0   0     s1
.24365000E+03  .67079000E+03  .20487500E+04  .71993200E+04  .31226800E+05
.20608200E+06
.29981000E+00  .12737000E+00  .39940000E-01  .98800000E-02  .19300000E-02
.25000000E-03
 2   2 01   2   0   0     s2
.39810100E+02  .95925000E+02
.23582000E+00  .41825000E+00
 3   1   1   1   0   0     s3
.12220500E+02
.10000000E+00
 4   1   1   1   0   0     s4
.50088200E+01
.10000000E+00
 5   1   1   1   0   0     s5
.12856900E+01
.10000000E+00
 6   1   1   1   0   0     s6
.51280600E+00
.10000000E+00
 7   1   1   1   0   0     s7
.85576000E-01
.10000000E+00
 8   1   1   1   0   0     s8
.33020000E-01
.10000000E+00


 9   4   2   4   0   0     p1
.36372700E+02  .96977700E+02  .30123000E+03  .12647000E+04
.24143000E+00  .81170000E-01  .17250000E-01  .21400000E-02
10   2   2   2   0   0     p2
.62746500E+01  .14781400E+02
.35714000E+00  .42631000E-00
11   1   2   1   0   0     p3
.24787800E+01
.10000000E+00
12   2   2   2   0   0     p4
.39816200E+00  .10161800E+01
.29986000E+00  .57709000E+00
13   1   2   1   0   0     p5
.6
1.0
14   1   2   1   0   0     p6
.3
1.0
15   1   2   1   0   0     p7
.08
1.0
16   1   2   1   0   0     p8
.03
1.0
```

```
17   4   4   4   0   0     d1
.80019800E+00  .23487100E+01  .70863400E+01  .25992400E+02
.60288000E+00  .42282000E+00  .15466000E+00  .29130000E-01
18   1   4   1   0   0     d2
.26204900E+00
.10000000E+00
19   1   4   1   0   0     d3
.72000000E-01
.10000000E+00
```

(5) O (s, p)

```
24   3   1   2   0   0     (O s1)
290.8205       1424.0643      4643.4485
 1.          0.1344         0.0323
25   4   1   2   0   0     (O s2)
 4.6037        12.8607        31.3166        76.232
 1.0838        1.8781         1.             0.6261
26   2   1   2   0   0     (O s3)
 0.9311        9.7044
 1.1526       -0.1538
27   1   1   1   0   0     (O s4)
 0.2825
 1.
28   1   1   1   0   0     (O s5)
 0.08
 1.

29   4   2   2   1   0     (O 2p1)
 0.7031        2.3606         9.0369         46.2879
202.777        84.9397        15.7917        1.
 0.0756        0.0641         0.0501         0.0417
 0.7031        3.6
202.777        90.101
 0.0756        0.0641
30   1   2   1   1   0     (O 2p2)
 0.212
 1.
 0.1178
 0.212
 1.
 0.1178
31   1   2   1   0   0     (O 3p1)
 0.08
 1.
 0.08
 1.
```

Appendix B

Zr Core Potential And Simplified Atomic Orbitals (exponent/coefficient)

```
   1  10   0  10   0   2                                    1s
0.16769577E+01 0.31369765E+01 0.64365559E+01 0.19458012E+02 0.44331005E+02
0.11895280E+03 0.27452888E+03 0.66301410E+03 0.17286244E+04 0.50459795E+04
0.12397320E-01-0.17764780E-01 0.16008200E-01-0.18858670E-01 0.17098290E-01
-0.22187415E+0-0.34779457E+00-0.37900190E+00-0.11381321E+00-0.84512380E-01
   2  10   0  10   0   2                                    2s
0.16769577E+01 0.31369765E+01 0.64365559E+01 0.19458012E+02 0.44331005E+02
0.11895280E+03 0.27452888E+03 0.66301410E+03 0.17286244E+04 0.50459795E+04
-0.21362850E-01 0.36143050E-01-0.79556050E-01-0.55881730E+0-0.56630793E+00
0.12233175E+00 0.21967778E+00 0.15275242E+00 0.41691940E-01 0.27872880E-01
   3  10   0  10   0   2                                    3s
0.16769577E+01 0.31369765E+01 0.64365559E+01 0.19458012E+02 0.44331005E+02
0.11895280E+03 0.27452888E+03 0.66301410E+03 0.17286244E+04 0.50459795E+04
-0.74857150E-01-0.60676303E+00-0.63785940E+00 0.53215640E+0 0.40851867E+00
-0.67174610E-01-0.98401100E-01-0.67182040E-01-0.17601200E-01-0.1178785E-01
   4  10   1   3   0   0                                    4s
0.35251601E+00 0.75794368E+00 0.16769577E+01 0.31369765E+01 0.64365559E+01
0.19458012E+02 0.44331005E+02 0.11895280E+03 0.27452888E+03 0.66301410E+03
0.41627810E+00 0.82381333E+00 0.10852728E+00-0.64826602E+00-0.37125336E+00
0.22637564E+00 0.16007664E+00-0.23661710E-01-0.32818370E-01-0.21576640E-01
   5  10   1   3   0   0                                    5s
0.16769577E+01 0.31369765E+01 0.64365559E+01 0.19458012E+02 0.44331005E+02
0.11895280E+03 0.27452888E+03 0.66301410E+03 0.17286244E+04 0.50459795E+04
0.24175050E-01-0.19806955E+00-0.11322635E+00 0.65587880E-01 0.45236440E-01
-0.67413400E-02-0.95584800E-02-0.63297800E-02-0.16360800E-02-0.1086940E-02
   6   1   1   1   0   0                                    5s'
 0.75794368E+00
 0.10000000E+01
 0.75794368E+00
 0.10000000E+01
  32   1   1   1   0   0                                    5s’
 0.35251601E+00
 0.10000000E+01
  33   1   1   1   0   0                                    5s’
 0.72983731E-01
 0.10000000E+01
  34   1   1   1   0   0                                    5s’
 0.28630798E-01
 0.10000000E+01




   7   6   1   6   0   2                                    2p
0.16539778E+01 0.42470841E+01 0.98279363E+01 0.23613474E+02 0.52676385E+02
0.12497249E+03
0.35956820E-01-0.64519800E-01 0.47578330E-01-0.47669277E+00-0.26403418E+00
-0.40986927E+00
   8   6   1   6   0   2                                    3p
0.16539778E+01 0.42470841E+01 0.98279363E+01 0.23613474E+02 0.52676385E+02
0.12497249E+03
-0.15727632E+00-0.54369901E+00-0.50029977E+00 0.18580162E+0 0.14723229E+00
 0.19241701E+00
```

```
   9   5   2   3   0   0                                      4p
0.42470841E+01 0.98279363E+01 0.23613474E+02 0.52676385E+02 0.12497249E+03
-0.31202773E+0-0.24376409E+00 0.78609630E-01 0.63892710E-01 0.83223960E-01
  10   2   2   2   0   0                                      4p'
0.71245766E+00 0.16539778E+01
0.70426270E+00 0.17106071E+00
   19.65753309   19.65753309    0.71245766
  11   1   2   1   0   0                                      4p"
0.27571726E+00
0.28258425E+00


  12   5   2   5   0   2                                      3d
0.11671223E+00 0.35016420E+00 0.27336987E+01 0.65072003E+01 0.15823177E+02
-0.57256200E-02 0.16695960E-01 0.37173270E+00 0.34196629E+0 0.46912482E+00
  13   4   4   4   0   0     4d1
 0.65072003E+01 0.15823177E+02 0.42117280E+02 0.14405409E+03
 0.44585293E+00 0.35708594E+00 0.14709321E+00 0.25712189E-01
  14   1   4   1   0   0     4d2
 0.27336987E+01
 0.10000000E+01
  35   1   4   1   0   0     4d3
 0.97846411E+00
 0.10000000E+01
  36   1   4   1   0   0     4d4
 0.35016420E+00
 0.10000000E+01
  37   1   4   1   0   0     4d5
 0.11671223E+00
 0.10000000E+01



  16   8   1   0   0   0      (Zr 1s-3d core)
0.15556020E+01 0.35095602E+01 0.10686120E+02 0.19401199E+02 0.68310600E+02
0.15317720E+03 0.55090400E+03 0.15420560E+04
0.48175530E+00-0.37579930E+01-0.50913631E+01 0.13432362E+01-0.33329932E+00
-0.83032708E-01 0.11723983E-01-0.99383946E-02
```

Oxygen Core Potential And Simplified Atomic Orbitals (exponent/coefficient)

```
  28   8   1   0   0   0      (O 1s-2p core)
0.41524000E+00 0.15556020E+01 0.35095602E+01 0.10686120E+02 0.19401199E+02
0.68310600E+02 0.15317720E+03 0.55090400E+03
-0.12995698E+02-0.19358549E+01-0.67225464E+00 0.27211981E+0-0.24564583E+00
-0.37039962E-01-0.52883028E-02-0.48219762E-03


  29  10   0  10   0   2      (O 1s )
0.80000000E-01 0.28250000E+00 0.93110000E+00 0.46037000E+01 0.97044000E+01
0.12860700E+02 0.31316600E+02 0.76232000E+02 0.29082050E+03 0.14240643E+04
0.42879000E-03-0.87810000E-03 0.83520700E-02 0.24474734E+00 0.31379600E-01
0.42686322E+00 0.24080091E+00 0.14901451E+00 0.46350780E-01 0.62299900E-02
  30  10   0  10   0   2      (O 2s )
0.80000000E-01 0.28250000E+00 0.93110000E+00 0.46037000E+01 0.97044000E+01
0.12860700E+02 0.31316600E+02 0.76232000E+02 0.29082050E+03 0.14240643E+04
-0.94609510E-01-0.49923834E+00-0.54878268E+00 0.46162620E-01
0.13202776E+00
0.59785680E-01 0.70515680E-01 0.33238590E-01 0.10462230E-01 0.13328000E-02
0.80000000E-01 0.28250000E+00 0.93110000E+00 0.46037000E+01 0.97044000E+01
  31   6   1   6   0   2      (O 2p )
0.80000000E-01 0.21200000E+00 0.70310000E+00 0.23606000E+01 0.90369000E+01
0.46287900E+02
0.32196914E+00 0.28322747E+00 0.40551237E+00 0.25700146E+00 0.73418000E-01
0.87357000E-02
```